Numerical analysis of the factorization method for EIT with a piecewise constant uncertain background

Houssem Haddar, Giovanni Migliorati

Numerical analysis of the Factorization Method for EIT with piece-wise constant uncertain background

Houssem Haddar[♯]   **Giovanni Migliorati**[♯†]

[♯]INRIA Saclay Ile de France and Ecole Polytechnique (CMAP) Route de Saclay, 91128, Palaiseau, France.
[†]Dipartimento di Matematica, Politecnico di Milano, Italy.

E-mail: `giovanni.migliorati@gmail.com`

Abstract.   We extend the Factorization Method for Electrical Impedance Tomography to the case of background featuring uncertainty. We first describe the algorithm for known but inhomogeneous backgrounds and indicate expected accuracy from the inversion method through some numerical tests. Then we develop three methodologies to apply the Factorization Method to the more difficult case of piece-wise constant but uncertain background. The first one is based on a recovery of the background through an optimization scheme and is well adapted to relatively low dimensional random variables describing the background. The second one is based on a weighted combination of the indicator functions provided by the Factorization Method for different realizations of the random variables describing the uncertain background. We show through numerical experiments that this procedure is well suited to the case where many realizations of the measurement operators are available. The third strategy is a variant of the previous one when measurements for the inclusion-free background are available. In that case, a single pair of measurements is sufficient to achieve comparable accuracy to the deterministic case.

1. Introduction

The problem of *Electrical Impedance Tomography* (EIT) arises in many applied contexts. It leads to well established operative procedures, *e.g.* in geophysics, nondestructive testing or imaging applications, while in other fields its usage is still experimental *e.g.* medicine, [1, 2, 3, 4, 5].

For some key theoretical results related to uniqueness and conditional stability of the EIT inverse problem, we refer to [6, 7, 8, 9] and references therein. On the numerical side, many mathematical models and inversion algorithms for EIT were proposed in the literature, trying to take into account as many physical phenomena as possible, see [1] and the references therein for a complete overview. In this work we address the so-called Factorization Method (FM) as introduced in [10] applied to the *Continuous Model* (CM) (in contrast with the so-called complete electrode model [11, 12]) in the context of EIT

featuring an inhomogeneous isotropic background. We shall in particular address the case where the inhomogeneous background cannot be considered as a small perturbation of the homogeneous one (as in [13]) and more importantly consider the case where this background is piecewise constant but with uncertain values on the conductivity (and not on the spatial distribution). The latter configuration is motivated by medical imaging experiments since the conductivity support may be known from the use of other imaging modalities, while the physical electrical parameters cannot be exactly determined.

Most of the works on the FM in the literature treat the case of homogeneous background, *e.g.* [14, 15]. Our work is mostly related to numerical issues associated with EIT in inhomogeneous and uncertain background. To begin with, we propose a numerical scheme to solve the dipole-like Neumann boundary-value problem when the background coefficient is inhomogeneous and deterministic, and use this scheme to design an efficient implementation of the FM algorithm for inhomogeneous but deterministic background. We then discuss the case where the background is piecewise constant with known spatial distribution but unknown parameter values. We propose three variants of the FM to cope with this configuration. In the first algorithm, by means of an optimization scheme motivated by the structure of the sampling operator and the outcome of the FM, we simultaneously recover the background parameters and the shape of the inclusion. This algorithm is well suited for low dimensional configurations of the parameter space, and can be applied to moderately high dimensional configurations by means of acceleration with polynomial approximation techniques [16, 17, 18]. In addition, an alternative approach is proposed, where the optimization scheme is replaced by a weighting of the FM indicator function with a misfit indicator for the background. This procedure requires an extensive sampling of the parameter space which would be very expensive. However, in the case where many independent realizations of the measurement operator are available, we describe how this strategy can be made efficient. The third algorithm deals with the case where paired measurements are available, namely measurements for the inclusion free background and measurements for the medium with inclusion. In this case, a uniform weight for the FM associated with random sampling of the parameter spaces provides an effective indicator function.

The outline of the paper is the following: in Section 2.1 we present the problem of EIT and the notation. In Section 2.2 we introduce the FM in deterministic inhomogeneous background and the numerical scheme proposed to solve the dipole-like singular problem. Then in Section 2.3 we describe the regularization technique employed. In Section 3 we introduce the problem of EIT in random media, starting from the parametrization of the background coefficient by random variables. A justification of how randomness affects the spectrum of the measurement operator is provided. Moreover, two situations are identified depending on how the measurements are collected, *i.e.* arbitrary or paired measurements. In Section 3.1 two variants of the FM are proposed, in the case of arbitrary measurements. In Section 3.2 a variant of the FM is proposed in the case of paired measurements. Sections 4, 5, 6 illustrate the performance of the variants of the FM proposed through several testcases. Finally, in

Section 7 we draw some conclusions.

2. The EIT problem and the Factorization Method

2.1. Mathematical formulation of the EIT problem

Consider a bounded Lipschitzian domain $B \subset \mathbb{R}^2$ and its subset $D \subset B$. We assume that D is a union of possibly disjoint Lipschitzian domains, each one with positive measure, and that $B \setminus \overline{D}$ is connected. The domain B represents the background medium, featured by the physical coefficient σ_B. The domain D represents an inclusion, displaced somewhere inside B. The inclusion is characterized by unknown shape and unknown value of its physical coefficient σ_D. We shall assume that σ_B and σ_D are real valued functions.

Now consider the coefficient $\sigma(x) \in L^\infty(B)$ defined as

$$\sigma(\mathbf{x}) = \begin{cases} \sigma_B(\mathbf{x}), & \text{in } B \setminus D, \\ \sigma_D(\mathbf{x}), & \text{in } D, \end{cases} \tag{1}$$

and define the functional spaces $\mathring{L}^2(\partial B)$, $\mathring{H}^1(B)$, $\mathring{H}^{\frac{1}{2}}(\partial B)$ and $\mathring{H}^{-\frac{1}{2}}(\partial B)$ as the subspaces of respectively $L^2(\partial B)$, $H^1(B)$, $H^{\frac{1}{2}}(\partial B)$ and $H^{-\frac{1}{2}}(\partial B)$ of functions with zero (boundary) mean value on ∂B.

Given $g \in \mathring{H}^{-\frac{1}{2}}(\partial B)$, consider the Neumann boundary-value problem, $u \in \mathring{H}^1(B)$ such that

$$\begin{cases} \nabla \cdot (\sigma(\mathbf{x})\nabla u) = 0, & \text{in } B, \\ \sigma(\mathbf{x})\nabla u \cdot \boldsymbol{\nu} = g, & \text{on } \partial B, \end{cases} \tag{2}$$

where $\boldsymbol{\nu}$ denotes the outward normal to ∂B. It is well known that problem (2) has a unique solution if $\sigma \in L^\infty(B)$ and is positive definite. In the case of the continuous EIT model, one prescibes a current pattern g and measures the generated potential $f = u|_{\partial B}$ on the boundary ∂B. The final aim is to retrieve some information about D, *e.g.* its location inside B and its shape.
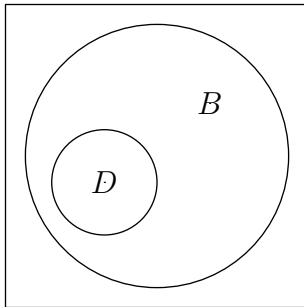
Fig. 1. An obstacle D which lies in a medium B.

The operator Λ that maps currents g into potentials f is the *NtDm* associated to problem (2) with coefficient (1). It is a continuos operator from $\mathring{H}^{-\frac{1}{2}}(\partial B)$ to $\mathring{H}^{\frac{1}{2}}(\partial B)$.

Denote also by Λ_0 the *NtDm* for the problem (2) with the coefficient

$$\sigma(\mathbf{x}) = \sigma_B(\mathbf{x}), \text{ in } B, \tag{3}$$

and by u_0 the solution of the same problem. In this way u_0 represents the potential generated by the incoming current g in the domain B, when the inclusion D is not present. Let f_0 be the corresponding measured potential $f_0 = u_0|_{\partial B} = \Lambda_0 g$. Both the operators Λ and Λ_0 are weakly compact, when restricted on $\mathring{L}^2(\partial B)$, *i.e.* $\Lambda : \mathring{L}^2(\partial B) \to \mathring{L}^2(\partial B)$ and $\Lambda_0 : \mathring{L}^2(\partial B) \to \mathring{L}^2(\partial B)$. Moreover, we define the operator $\widetilde{\Lambda}$

$$\widetilde{\Lambda} := \Lambda - \Lambda_0 : \mathring{L}^2(\partial B) \to \mathring{L}^2(\partial B), \tag{4}$$

that has the remarkable property of being strongly compact (eigenvalues decay exponentially fast: see for instance (32)).

We will need also the Green function $N(\cdot, \boldsymbol{\xi}) \in \mathring{L}^2(B)$, which is a solution of the following Neumann boundary-value problem with a Dirac source δ_ξ centered in $\boldsymbol{\xi} \in B$:

$$\begin{cases} \nabla_1 \cdot (\sigma_B(\mathbf{x}) \nabla_1 N(\mathbf{x}, \boldsymbol{\xi})) = -\delta_\xi(\mathbf{x}), & \mathbf{x} \in B, \\ \boldsymbol{\nu} \cdot \sigma_B(\mathbf{x}) \nabla_1 N(\mathbf{x}, \boldsymbol{\xi}) = -\frac{1}{|B|}, & \mathbf{x} \text{ on } \partial B. \end{cases} \tag{5}$$

Note that (5) does not embed any information about the inclusion D. Denote by $\mathbf{p}$ a two-dimensional versor (*i.e.* $|\mathbf{p}| = 1$). In the sequel we will often need the test function

$$\psi(\mathbf{x}, \boldsymbol{\xi}, \mathbf{p}) := \mathbf{p} \cdot \nabla_2 N(\mathbf{x}, \boldsymbol{\xi}), \quad \mathbf{x} \in B, \tag{6}$$

as well as its restriction on ∂B

$$l_\xi^p = \psi(\mathbf{x}, \boldsymbol{\xi}, \mathbf{p}) \Big|_{\mathbf{x} \text{ on } \partial B}. \tag{7}$$

Moreover, denoting with $\{\mathbf{e}_1, \mathbf{e}_2\}$ an orthonormal basis of $\mathbb{R}^2$, we define

$$l_\xi^k = l_\xi^{e_k}, \quad k = 1, 2.$$

Remark 1 *When the domain B is a circle with radius R there is an explicit formula for the solution $N(\mathbf{x}, \boldsymbol{\xi})$ of the Neumann problem (5) with $\sigma_B \equiv 1$ (see e.g. [19]):*

$$N(\mathbf{x}, \boldsymbol{\xi}) = -\frac{1}{2\pi} \left(\log |\mathbf{x} - \boldsymbol{\xi}| + \log \left| \frac{R}{|\mathbf{x}|} \mathbf{x} - \frac{|\mathbf{x}|}{R} \boldsymbol{\xi} \right| \right) + \frac{\log R}{\pi}. \tag{8}$$

In this case we have an explicit formula for the evaluation of ψ defined in (6) on the boundary of the unitary circle :

$$\psi(\mathbf{x}, \boldsymbol{\xi}, \mathbf{p}) \Big|_{\partial B} = \frac{1}{\pi} \frac{\mathbf{p} \cdot (\boldsymbol{\xi} - \mathbf{x})}{|\boldsymbol{\xi} - \mathbf{x}|^2}, \quad for \ |\mathbf{x}| = 1. \tag{9}$$

2.2. The Factorization Method with deterministic inhomogeneous background

In this section we outline the basis of the FM applied to EIT and some numerical issues related to the case of inhomogeneous background. The main result that motivates the FM algorithm is Theorem (1). It provides a necessary and sufficient criterion to localize a point inside the support of the inclusions. Remark 2 shows how this criterion becomes operative. This theorem can be proved following the lines of the proof of [10, Theorem

6.8] that treats the case of constant σ_B (see also [19]). The only point that requires attention is the use of unique continuation arguments for equations of type (2), and this is why a regularity assumption on σ_B is required.

Assumption 1 *Assume σ and σ_B are bounded and positive definite functions on B and that σ_B is piecewise Lipschitz continuous and with Lipschitz discontinuity interfaces. Moreover, denoting by*

$$\sigma_B^m = \min_{x \in D} \sigma_B(\mathbf{x}) \quad and \quad \sigma_B^M = \max_{x \in D} \sigma_B(\mathbf{x}),$$

then σ_B and σ_D satisfy

$$\sigma_D(\mathbf{x}) < \sigma_B^m - \delta \quad or \quad \sigma_B^M < \sigma_D(\mathbf{x}) - \delta$$

a.e. in D, for some positive constant δ.

Theorem 1 *Assume that assumption (1) holds. Then the operator $\widetilde{\Lambda} : \mathring{L}^2(\partial B) \to \mathring{L}^2(\partial B)$ is self adjoint and injective. Moreover, for any versor p*

$$l_\xi^p \in Range(|\widetilde{\Lambda}|^{1/2}) \iff \boldsymbol{\xi} \in D.$$

Remark 2 *Denote by $\{\lambda_j, w_j : j \in J\}$ the spectral system of the self adjoint and compact operator $\widetilde{\Lambda}$. Then*

$$w \in Range(|\widetilde{\Lambda}|^{1/2}) \iff \sum_{j=1}^\infty \frac{|(w, w_j)_{L^2(\partial B)}|^2}{|\lambda_j|} < \infty. \tag{10}$$

The main difficulty in implementing the FM for inhomogeneous background is the precise evaluation of l_ξ^p that can only be done in the general case by numerically solving problem (5). To overcome the singularity in the forcing term, we resort to the fundamental solution

$$\phi(\cdot, \boldsymbol{\xi}) = -\frac{1}{2\pi\sigma_B(\boldsymbol{\xi})} \log\left|\cdot - \boldsymbol{\xi}\right|, \quad \mathbf{x} \in \mathbb{R}^2, \tag{11}$$

of the problem

$$-\nabla \cdot \left(\sigma_B(\boldsymbol{\xi})\nabla\phi(\cdot, \boldsymbol{\xi})\right) = \delta_\xi, \quad \text{in } \mathbb{R}^2. \tag{12}$$

Since the singularity at $\boldsymbol{\xi}$ in problem (5) is of the same kind as in problem (12), we can restrict problem (5) in a small neighbourhood $\mathcal{O}(\boldsymbol{\xi}) \subset \mathbb{R}^2$ of $\boldsymbol{\xi}$ where

$$\sigma_B(\mathbf{x}) \approx \sigma_B(\boldsymbol{\xi}), \quad \forall \mathbf{x} \in \mathcal{O}(\boldsymbol{\xi}),$$

and approximate the solution $N(\mathbf{x}, \boldsymbol{\xi})$ of problem (5) near the singularity in $\boldsymbol{\xi}$ as

$$N(\mathbf{x}, \boldsymbol{\xi}) \approx \phi(\mathbf{x}, \boldsymbol{\xi}), \quad \forall \mathbf{x} \in \mathcal{O}(\boldsymbol{\xi}). \tag{13}$$

Then it is possible to write a nonsingular problem for the difference

$$\varphi_N(\cdot, \boldsymbol{\xi}) = N(\cdot, \boldsymbol{\xi}) - \phi(\cdot, \boldsymbol{\xi}), \tag{14}$$

plugging (14) in (5). The quantity $\psi(\cdot, \boldsymbol{\xi}, \mathbf{p})$ defined in (6) is a solution of problem (5) for any $\mathbf{p}$. Moreover, in ψ the dependece of $N(\cdot, \cdot)$ on the second argument is smooth.

So we can exploit this regularity to derive a numerical scheme that given $\boldsymbol{\xi} \in B$ directly computes $\nabla_2 N(\cdot, \boldsymbol{\xi})$, that is needed to obtain l_ξ^p through ψ and apply Theorem 1. To this aim we differentiate (14) with respect to the second argument, and obtain

$$\nabla_2 \varphi_N(\cdot, \boldsymbol{\xi}) = \nabla_2 N(\cdot, \boldsymbol{\xi}) - \nabla_2 \phi(\cdot, \boldsymbol{\xi}). \tag{15}$$

The derivatives of ϕ w.r.t. $\boldsymbol{\xi}$ are

$$\frac{\partial \phi(\cdot, \boldsymbol{\xi})}{\partial \xi_k} = \frac{1}{2\pi \sigma_B(\boldsymbol{\xi})^2} \frac{\partial \sigma_B(\boldsymbol{\xi})}{\partial \xi_k} \log\left(|\mathbf{x} - \boldsymbol{\xi}|\right) + \frac{x_k - \xi_k}{2\pi \sigma_B(\boldsymbol{\xi})|\mathbf{x} - \boldsymbol{\xi}|^2}, \quad k = 1, 2,$$

and since ϕ is analytical when $\mathbf{x} \neq \boldsymbol{\xi}$ then the mixed derivatives coincide:

$$\frac{\partial^2 \phi(\mathbf{x}, \boldsymbol{\xi})}{\partial x_k \partial \xi_k} = \frac{1}{2\pi \sigma_B(\boldsymbol{\xi})^2} \frac{\partial \sigma_B(\boldsymbol{\xi})}{\partial \xi_1} \frac{x_k - \xi_k}{|\mathbf{x} - \boldsymbol{\xi}|^2} + \frac{|\mathbf{x} - \boldsymbol{\xi}|^2 - 2(x_k - \xi_k)^2}{2\pi \sigma_B(\boldsymbol{\xi})|\mathbf{x} - \boldsymbol{\xi}|^4},$$

$$\frac{\partial^2 \phi(\mathbf{x}, \boldsymbol{\xi})}{\partial x_\ell \partial \xi_k} = \frac{1}{2\pi \sigma_B(\boldsymbol{\xi})^2} \frac{\partial \sigma_B(\boldsymbol{\xi})}{\partial \xi_1} \frac{x_\ell - \xi_\ell}{|\mathbf{x} - \boldsymbol{\xi}|^2} - \frac{(x_k - \xi_k)(x_\ell - \xi_\ell)}{\pi \sigma_B(\boldsymbol{\xi})|\mathbf{x} - \boldsymbol{\xi}|^4},$$

for $k, \ell = 1, 2$ and $\ell \neq k$. Denoting by superscript the partial derivative, we have two problems for the unknowns $\varphi_N^k = \partial \varphi_N / \partial \xi_k$, $k = 1, 2$:

$$\begin{cases} -\nabla_x \cdot \left(\sigma_B(\mathbf{x})\nabla_1 \varphi_N^k(\mathbf{x}, \boldsymbol{\xi})\right) = -\nabla_x \cdot \left(\left(\sigma_B(\boldsymbol{\xi}) - \sigma_B(\mathbf{x})\right)\boldsymbol{\Phi}^k(\mathbf{x}, \boldsymbol{\xi})\right), & \mathbf{x} \text{ in } B, \\ \sigma_B(\mathbf{x})\nabla_1 \varphi_N(\mathbf{x}, \boldsymbol{\xi}) \cdot \boldsymbol{\nu} = -\sigma_B(\mathbf{x})\boldsymbol{\Phi}^k(\mathbf{x}, \boldsymbol{\xi}) \cdot \boldsymbol{\nu} - \frac{1}{|\partial B|}, & \mathbf{x} \text{ on } \partial B, \end{cases} \tag{16}$$

with

$$\boldsymbol{\Phi}^k(\mathbf{x}, \boldsymbol{\xi}) = \left(\frac{\partial^2 \phi(\mathbf{x}, \boldsymbol{\xi})}{\partial x_1 \partial \xi_k}, \frac{\partial^2 \phi(\mathbf{x}, \boldsymbol{\xi})}{\partial x_2 \partial \xi_k}\right), \qquad \forall (\mathbf{x}, \boldsymbol{\xi}) \in B \times B : \mathbf{x} \neq \boldsymbol{\xi}.$$

All the second derivatives of ϕ are singular in $\mathbf{x} = \boldsymbol{\xi}$, and behave like $1/|\mathbf{x} - \boldsymbol{\xi}|^2$. Therefore if $\sigma_B(\cdot)$ is piecewise Lipschitz then the solution of (16) is in $H^1(B)$. Hence the variational formulation of (16) is suited for standard finite element discretizations. Once the solution of (16) has been computed, then $\nabla_2 N(\cdot, \boldsymbol{\xi})$ can be recovered from (15). Note that when σ_B is piece-wise constant and $\boldsymbol{\xi}$ does not fall where it jumps, the function $\zeta(\mathbf{x}, \boldsymbol{\xi}) = \sigma_B(\boldsymbol{\xi}) - \sigma_B(\mathbf{x})$ vanishes as $\mathbf{x}$ approaches $\boldsymbol{\xi}$.

2.3. Description of the algorithm for the deterministic setting

Now we present our operative criterion to implement the range test. It is based on the spectral decomposition of the operator $|\widetilde{\Lambda}|^{1/2}$ and on the use of an appropriate regularization. We focus mainly on *Tikhonov Regularization* (TR), although also a straightforward application of the *Picard Criterion* (23) can give good results when the background is homogeneous (see Remark 3 below). To simplify the notation we set $M = |\widetilde{\Lambda}|^{1/2}$. To check whether a given l_ξ^k belongs to Range(M) we have to solve the problem

$$M g_\xi^k = l_\xi^k, \tag{17}$$

which demands for regularization. The keypoint is

$$\boldsymbol{\xi} \in D \quad \Longleftrightarrow \quad \left(\|g_\xi^k\|_{L^2(\partial B)}\right)^{-1} = 0.$$

The TR of (17) reads

$$\left(\alpha + M^*M\right)g_\xi^k = M^*l_\xi^k. \tag{18}$$

We choose the *Fourier basis* to discretize the operator M. Since we discretize l_ξ^k and g_ξ^k in (17) over the same orthogonal basis, then the discretization of M is a square matrix.

In the sequel we denote by σ_i the singular values of M and by u_i and v_i the corresponding left and right singular vectors. Both the sets $\{u_i\}_{i=1}^\infty$ and $\{v_i\}_{i=1}^\infty$ form an orthonormal basis of $L^2(\partial B)$. The regularized solution of problem (18) is

$$g_\xi^k = \sum_{i=1}^\infty \frac{\sigma_i}{\alpha + \sigma_i^2}(l_\xi^k, u_i)v_i. \tag{19}$$

We choose the regularization parameter α using *Morozov principle, i.e.* imposing

$$\|Mg_\xi^k - l_\xi^k\|_{L^2(\partial B)} = \delta, \tag{20}$$

with the parameter $\delta > 0$ to be in some way related to the accuracy of the measurements. We pick

$$\delta = \gamma\sigma_1, \tag{21}$$

being σ_1 the largest singular value of M, and γ a given threshold. The terms l_ξ^k depends on ξ, so to ensure that (20) is uniformly satisfied we normalize l_ξ^k as $\hat{l}_\xi^k = l_\xi^k/\|l_\xi^k\|_{L^2(\partial B)}$. The optimal value of α is computed plugging (19) into the nonlinear equation (20), and solving with respect to α. To show the inversion results, we display the isolines of the indicator function

$$C(\boldsymbol{\xi}) = \left(\log\left(v_1(\boldsymbol{\xi}) + v_2(\boldsymbol{\xi})\right)\right)^{-1}, \tag{22}$$

where $v_k(\boldsymbol{\xi}) := \|g_\xi^k\|_{L^2(\partial B)}$. We can summarize the algorithm by the following:

Algorithm 1 The Factorization Method in inhomogeneous deterministic background

---

Sample the region of B to be probed with a set of points $\mathcal{P} = \{\boldsymbol{\xi}_j\}_{j=1}^P$
for $\boldsymbol{\xi}$ in the set $\mathcal{P}$ **do**
   solve problem (5) to find its solution $N(\cdot, \boldsymbol{\xi})$,
   compute l_ξ^k from $N(\cdot, \boldsymbol{\xi})$ using (7),
   use $l_{\boldsymbol{\xi}}^k$ to compute the indicator $C(\boldsymbol{\xi})$ in (22),
   plot $\boldsymbol{\xi} \mapsto C(\boldsymbol{\xi})$.
end for

Remark 3 (Picard criterion) *Another criterion to test the range condition is analyzed in [20]. It employs the indicator function:*

$$I_k(\boldsymbol{\xi}) = \frac{1}{\|l_\xi^k\|_{L^2(\partial B)}^2} \sum_{i=1}^\infty \frac{\left|(l_\xi^k, u_i)_{L^2(\partial B)}^2\right|^2}{|\sigma_i|}, \tag{23}$$

and it reads $\boldsymbol{\xi} \in D \iff I_k(\boldsymbol{\xi}) < \infty$. *Note that the normalization of* l_{ξ}^k *is already embedded in (23). We refer to this criterion as* Picard Criterion (PC). *It does not require to solve problem (17) to find its regularized solution. However, as discussed in [21], the regularization technique TR is more accurate than PC when the background is not homogeneous, above all in presence of many inclusions. Hence, in this paper we present only the results obtained using the TR technique. See also [21] for a comparison between TR and PC for several numerical examples.*

We consider backgrounds that are piece-wise constant in r regions $\{R_i\}_{i=1}^r$ that are a partition of unity of the computational domain $B = \bigcup_{i=1}^r R_i$, see *e.g.* Fig. 3. Denote by $\mathbf{m}$ the r-dimensional vector of positive numbers that specifies the coefficient value in each region R_i of the domain B. The background coefficient σ_B is defined as

$$\sigma_B(\mathbf{x}) = \sum_{i=1}^r m_i \, \mathbb{I}_{R_i}(\mathbf{x}), \qquad \mathbf{x} \in B, \tag{24}$$

where $\mathbb{I}_X(\mathbf{x})$ denotes the indicator function of the subdomain $X \subseteq B$. If $\boldsymbol{m}$ is the unitary vector then we obtain a homogeneous deterministic coefficient. Since σ_B is a diffusion coefficient, it has to be positive: therefore we assume that $m_i > 0$, $\forall i$. More general deterministic inhomogeneous coefficients σ_B, nonlinearly depending on $\mathbf{x}$, have been analyzed in [21]. The effect of noise has been analyzed in [21] as well.

3. The problem of EIT in random background

A natural issue that arises in the mathematical modeling of physical phenomena concerns the uncertainty in the input data. There are mainly two interpretations on how the presence of uncertainty in the model could be characterized: the epistemic and the aleatory interpretation. We introduce them directly in the context of EIT and the applications that we have in mind.

In the EIT framework the most natural choice to incorporate in the model the uncertainty affecting the background media is to consider the background coefficient σ_B as a random variable. In the epistemic uncertainty, we can imagine that the coefficient that models the background material is deterministic but unkwnown, because of the lack of knowledge or because of inaccurate measure instruments. Therefore we can model it as a random variable, although there are also other ways to cope with epistemic uncertainty. In the aleatory uncertainty, the coefficient is really random, according to a prescribed probability density. We could think of its realizations coming from a stationary or from a nonstationary stochastic process.

In general, the treatment of uncertainty through random variables distributed according to given probability densities is known as probabilistic approach. For any positive integer N, we introduce the N-dimensional parameter space $\Gamma \subseteq \mathbb{R}^N$, the probability density $\rho : \Gamma \to \mathbb{R}$ and the Hilbert space $L^2(\Gamma, d\rho)$ equipped with the inner product $\langle u, v \rangle = \sqrt{\int_\Gamma u(\mathbf{y}) \, v(\mathbf{y}) \, d\rho(\mathbf{y})}$. Denote by $\mathbf{Y} \sim \rho$ a multidimensional random variable, and by $\mathbf{y} \in \Gamma$ any of its realizations. We denote by $L^2(\Gamma, L^\infty(B))$ the Bochner

space of functions that take values into Γ and are $L^\infty(B)$-valued. Then we define the random diffusion coefficient $\sigma_B \in L^2(\Gamma, L^\infty(B))$ as

$$\sigma_B(\cdot, \mathbf{y}) \in L^\infty(B), \quad \forall\, \mathbf{y} \in \Gamma. \tag{25}$$

Moreover, we assume a smooth dependence of σ_B on $\mathbf{y}$:

Assumption 2 $\forall\, \mathbf{y} \in \Gamma$ *the map* $\mathbf{y} \mapsto \sigma(\cdot, \mathbf{y})$ *is assumed to be smooth (analytical).*

We will consider two parametrizations of the random coefficient σ_B introduced in (25). Again, the spatial background is piece-wise constant in r regions $\{R_i\}_{i=1}^r$ that are a partition of unity of the computational domain $B = \bigcup_{i=1}^r R_i$. The randomness concerns the value of the coefficient in each region R_i. We associate each component of the N-dimensional random variable $\mathbf{Y}$ to a region, hence $N = r$.

The first parametrization is suited for uncertainty analysis, and is an extension of (24) to the case of random background:

$$\sigma_B(\mathbf{x}, \mathbf{Y}) = \sum_{i=1}^r \left(m_i + d_i \cdot Y_i \right) \mathbb{I}_{R_i}(\mathbf{x}), \quad \mathbf{x} \in B, \quad \mathbf{Y} \in \Gamma = [-1, 1]^r. \tag{26}$$

The vectors $\boldsymbol{m}$ and $\boldsymbol{d}$ quantify the mean and dispersion of the coefficient in each region, and $m_1 = 1$, $d_1 = 0$. The range of variation in each region is $[m_i - d_i, m_i + d_i]$, and we have to assume that $m_i - d_i > 0$, $\forall\, i$, as we did for (24).

The second parametrization is suited for large variations of the background coefficient σ_B, and we parametrize it with the exponential model

$$\sigma_B(\mathbf{x}, \mathbf{Y}) = \sum_{i=1}^r 10^{Y_i} \mathbb{I}_{R_i}(\mathbf{x}), \quad \mathbf{x} \in B, \quad \mathbf{Y} \in \Gamma = [-1, 1]^r, \tag{27}$$

so that the coefficient jumps by two orders of magnitude in each one of the r regions.

Because of the randomness in σ_B, the diffusion coefficient (1) of problem (2) becomes random as well, and the solution $u = u(\mathbf{x}, \mathbf{Y})$ of (2) belongs to the space $\mathring{H}^1(B) \otimes L^2(\Gamma, d\rho)$ [16, 17, 18]. In the same way the Neumann-to-Dirichlet maps $\Lambda : \mathring{L}^2(\partial B) \otimes L^2(\Gamma, d\rho) \to \mathring{L}^2(\partial B) \otimes L^2(\Gamma, d\rho)$ and $\Lambda_0 : \mathring{L}^2(\partial B) \otimes L^2(\Gamma, d\rho) \to \mathring{L}^2(\partial B) \otimes L^2(\Gamma, d\rho)$ become random themselves. Also the Green function $N = (\mathbf{x}, \boldsymbol{\xi}, \mathbf{y}) \in D \otimes D \otimes \Gamma \mapsto N(\mathbf{x}, \boldsymbol{\xi}, \mathbf{y}) : D \otimes D \otimes \Gamma \to \mathring{L}^2(B) \otimes L^2(\Gamma, d\rho)$ depends on the random variable $\mathbf{Y}$ because it solves problem (5) with the random coefficient (25). For the same reason, the quantities (7) depend now on any realization $\mathbf{y} \in \Gamma$ of $\mathbf{Y}$,

$$l_\xi^p = l_\xi^p(\mathbf{y}), \qquad \forall\, \mathbf{y} \in \Gamma. \tag{28}$$

We define a measurement of the random operator Λ (or Λ_0) its observation for a single realization of the random variable $\mathbf{Y}$. In practice the measurements of Λ come from experiments, while the measurements of Λ_0 could be simulated numerically. We will always assume that it is not possible to recover the value of the realization of $\mathbf{Y}$ that generated the measurement of Λ, because this would reduce the inverse problem in random background to an inverse problem with deterministic background. Moreover, we need also the following assumption:

Assumption 3 *We assume to be able to evaluate the operator Λ for any realization of the random variable $\mathbf{Y}$. To evaluate the operator Λ means that we are able to collect all the voltages corresponding to the current patterns in the Fourier basis, up to a certain accuracy.*

This assumption is completely fine in the epistemic uncertainty or in the stationary aleatory uncertainty, but could not be the case in the nonstationary aleatory uncertainty.

Now we discuss the crucial point of how to extend to random background the operator $\widetilde{\Lambda}$ defined in (4) for inhomogeneous but deterministic background. The main question is: how do we collect the measurements of the random operators Λ and Λ_0? Denote by $\{\boldsymbol{y}_m\}$ and $\{\widehat{\boldsymbol{y}}_t\}$ the sets of unknown independent realizations of the random variable $\boldsymbol{Y}$ that generated the corresponding measurements of the random operator Λ and Λ_0, respectively. Even if the values of the realizations are unknown, at least two different situations can be identified, depending on how the measurements are collected:

- **arbitrary measurements**: the measurements of Λ and Λ_0 are collected separately, *i.e.* the sets $\{\boldsymbol{y}_m\}_m$ and $\{\widehat{\boldsymbol{y}}_t\}_t$ have nothing to do each other. In the sequel we need only to assume that the realizations in each set are independent only among those belonging to the same set.

- **paired measurements**: the measurements of Λ and Λ_0 are collected in pair, *i.e.* the mth measurement of Λ and Λ_0 is collected with the same (but unknown) realization $\boldsymbol{y}_m = \widehat{\boldsymbol{y}}_m$ of the random variable $\boldsymbol{Y}$.

The case of arbitrary measurements is the general one, and it arises in both epistemic and aleatory uncertainty. The case of paired measurements arises in epistemic uncertainty. For example, in crack testing: several mechanical objects are built together with the same internal but unknown properties. The measurements of Λ are collected using the mechanical object to test, and the measurements of Λ_0 are collected using a reference object, where the absence of cracks has been checked by means of other more expensive techniques.

When the measurements are paired, we can define the operator $\widetilde{\Lambda}$ in the case of random background as in (4),

$$\widetilde{\Lambda}(\boldsymbol{y}) = \Lambda(\boldsymbol{y}) - \Lambda_0(\boldsymbol{y}), \quad \boldsymbol{y} \in \Gamma, \tag{29}$$

where now the operator is parametrized by the realization $\boldsymbol{y} \in \Gamma$ of the random variable $\boldsymbol{Y}$. Therefore

$$\widetilde{\Lambda} : \mathring{L}^2(\partial B) \otimes L^2(\Gamma, d\rho) \to \mathring{L}^2(\partial B) \otimes L^2(\Gamma, d\rho),$$

and $\widetilde{\Lambda}(\boldsymbol{y}) : \mathring{L}^2(\partial B) \to \mathring{L}^2(\partial B)$ is strongly compact for any value $\boldsymbol{y} \in \Gamma$. At this point, the only difficulty that remains is that the value of $\boldsymbol{y}$ that generated the measurement is unknown. We will see in Section 3.2 how to cope with this issue.

When the measurements are arbitrary, the operator $\widetilde{\Lambda}$ depends on $\boldsymbol{y}$ and $\widehat{\boldsymbol{y}}$,

$$\widetilde{\Lambda}(\boldsymbol{y}, \widehat{\boldsymbol{y}}) = \Lambda(\boldsymbol{y}) - \Lambda_0(\widehat{\boldsymbol{y}}), \quad \boldsymbol{y}, \widehat{\boldsymbol{y}} \in \Gamma, \tag{30}$$

and the property of strongly compactness of the operator $\widetilde{\Lambda}(\boldsymbol{y}, \widehat{\boldsymbol{y}}) : \mathring{L}^2(\partial B) \to \mathring{L}^2(\partial B)$ is lost in general. However, we know that the singular values of a strongly compact operator decay exponentially fast. So we can look at the singular values of $\widetilde{\Lambda}$ as defined in (30), and choose the value of $\widehat{\boldsymbol{y}}$ that yields the fastest decay of the spectrum of $\widetilde{\Lambda}$. The singular values of several strongly compact operators are computed in [21].

We introduce the quantity K defined as

$$K(\boldsymbol{y}, \widehat{\boldsymbol{y}}) = \left| \text{supp}_{\boldsymbol{x} \in B} \left\{ |\sigma(\boldsymbol{x}, \boldsymbol{y}) - \sigma_B(\boldsymbol{x}, \widehat{\boldsymbol{y}})| \neq 0 \right\} \right|, \quad \boldsymbol{y}, \widehat{\boldsymbol{y}} \in \Gamma, \tag{31}$$

that gives the size of the support of the contrast between σ and σ_B, for any realization $\boldsymbol{y}$ and $\widehat{\boldsymbol{y}}$ in Γ. Of course

$$|D| = K(\boldsymbol{y}, \boldsymbol{y}) \leq K(\boldsymbol{y}, \widehat{\boldsymbol{y}}) \leq |B|, \quad \forall (\boldsymbol{y}, \widehat{\boldsymbol{y}}) \in \Gamma \times \Gamma.$$

In general, the singular values of $\widetilde{\Lambda}$ increase with respect to the value of K. The next remark proves this statement in a particular situation where explicit calculations are made possible.

Remark 4 *Suppose that B is a circular domain with unitary radius, and D is a concentric circular inclusion with radius $\rho < 1$. The diffusion coefficient is assumed to be homogeneous both in the background and in the inclusion. We define $\mu = \sigma_B / \sigma_D$ and observe that K defined in (31) satisfies $K = |supp_{\boldsymbol{x} \in B}\{\sigma - \sigma_B \neq 0\}| = |D|$. Of course we have $\rho^2 \propto K$. The eigenvalues of the Dirichlet-to-Neumann map defined by problem (2) satisfy (see also [22, Section 2] and [23, Lemma 4. 1])*

$$|\lambda_i^{DN}| = i \left| \frac{\mu + 1 - (\mu - 1)\rho^{2i}}{\mu + 1 + (\mu - 1)\rho^{2i}} \right|, \quad i = 1, 2, \ldots$$

and therefore the eigenvalues of the dual Neumann-to-Dirichlet map decay as

$$|\lambda_i^{ND}| = \frac{1}{i} \left| \frac{\mu + 1 + (\mu - 1)\rho^{2i}}{\mu + 1 - (\mu - 1)\rho^{2i}} \right|, \quad i = 1, 2, \ldots$$

From this we can derive the decay of the eigenvalues of the operator $\widetilde{\Lambda}$:

$$|\lambda_i(\widetilde{\Lambda})| = \frac{1}{i} \left| \frac{\mu + 1 + (\mu - 1)\rho^{2i}}{\mu + 1 - (\mu - 1)\rho^{2i}} - 1 \right| = \frac{1}{i} \left| \frac{2}{\rho^{-2i}(2(\mu - 1)^{-1} + 1) - 1} \right|, \quad i = 1, 2, \ldots \tag{32}$$

and clearly the smallest $\rho < 1$ the fastest the decay, as shown in Fig. 2. See also the numerical section where we tested inclusions with radius $\rho = 0.1$ and $\rho = 0.0275$. From (32), if we suppose $\mu > 1$ we derive

$$|\lambda_i^{ND}| \sim \frac{K^i}{i} \frac{\mu - 1}{\mu + 1}, \quad i = 1, 2, \ldots$$

The dependency on μ of the eigenvalues is very small, and it becomes unperceivable already from the third eigenvalue λ_3 on (see Fig. 2). Looking at the first eigenvalue we see a slight dependence of λ_1 on μ: the higher μ (that is equivalent to say the higher the contrast $\sigma_B - \sigma_D$) the slower the decay. The case $\rho = 0.1$ and $\mu = 10000$ has been tested in the numerical section, since we have set $\sigma_D = 10^{-4}$ and $\sigma_B \equiv 1$.
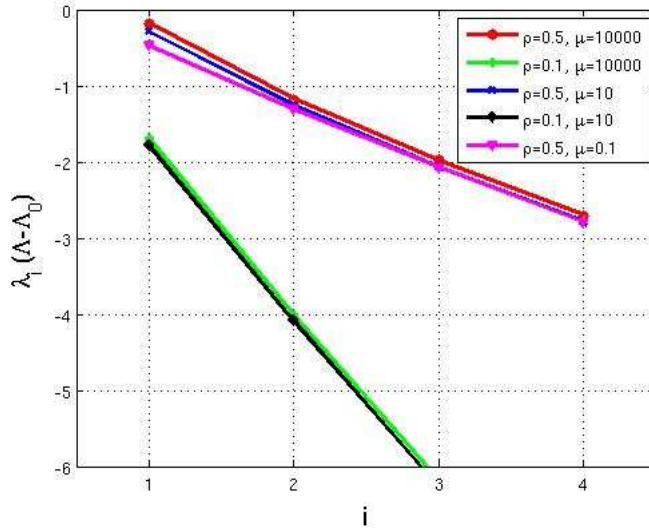
Fig. 2. The decay of the eigenvalues $\lambda_i(\widetilde{\Lambda})$ in (32) for different choices of ρ and μ.

Remark 5 *The same argument outlined in Remark 4 is useful to investigate also the case of piece-wise constants background with random values. Suppose that the circular domain B contains a concentric circular region R_2, and $R_1 = B \setminus R_2$. Consider $\sigma_B = 1$ in R_1 and $\sigma_B = y$ in R_2, where y is the realization of the random variable Y observed when getting the measurement of Λ. When we get the measurement of Λ_0 we observe another realization $\widehat{y}$ of the same random variable Y, so that $\sigma_B = 1$ in R_1 but $\sigma_B = \widehat{y}$ in R_2 and the region R_2 is generating a contrast $|y - \widehat{y}|$ in the diffusion coefficient of the operator $\widetilde{\Lambda}$. Therefore the region R_2 is behaving as an inclusion in the operator $\widetilde{\Lambda}$. The real inclusion lies in the center of the domain B, but is obfuscated from the presence of the contrast region R_2. Due to the presence of the inclusion, the region R_2 is slightly inhomogeneous in its center, but as explained in Remark 4 the value of the contrast is practically negligible compared to ρ.*

Remark 4 and Remark 5 justify analytically that the decay of the eigenvalues is slower, the larger is $K(\boldsymbol{y}, \widehat{\boldsymbol{y}})$ with respect to ρ. Formally $K(\boldsymbol{y}, \widehat{\boldsymbol{y}})$ can attain the value $|D|$, but when the random coefficient is associated to a continuous probability density a contrast is always present with probability one. The same occurs also in the applications: there is always a contrast somewhere in the domain between the background coefficient of Λ and Λ_0, because of modeling, measurement and numerical errors. As a consequence, the quantity K and the value of the contrast $|\sigma(\boldsymbol{x}, \boldsymbol{y}) - \sigma_B(\boldsymbol{x}, \widehat{\boldsymbol{y}})|$ have both influence on the decay of the eigenvalues. Since the background coefficients σ and σ_B are continuous w.r.t. the random variables (because of Assumption (2)), the magnitude of their contrast $|\sigma(\boldsymbol{x}, \boldsymbol{y}) - \sigma_B(\boldsymbol{x}, \widehat{\boldsymbol{y}})|$ satisfies

$$\sup_{\boldsymbol{x} \in B}|\sigma(\boldsymbol{x}, \boldsymbol{y}) - \sigma_B(\boldsymbol{x}, \widehat{\boldsymbol{y}})| \leq C\|\widehat{\boldsymbol{y}} - \boldsymbol{y}\|_\infty, \quad \forall\, (\boldsymbol{y}, \widehat{\boldsymbol{y}}) \in \Gamma \times \Gamma.$$

In conclusion, we proved that in a circular domain with a circular concentric inclusion and piece-wise constant background the decay of the eigenvalues of $\widetilde{\Lambda}$ is

governed by $\|\widehat{\boldsymbol{y}} - \boldsymbol{y}\|_\infty$. Reasonably the same conclusion can be extended to more general geometries and partitions of the domain into regions with arbitrary shape.

Consequently, when $M = 1$ and $\Lambda(\mathbf{y})$ is the only measurement generated by the (unknown) realization $\mathbf{y}$, we propose to solve the inverse problem

$$\widehat{\boldsymbol{y}} = \underset{\boldsymbol{y}^* \in \Gamma}{\operatorname{argmin}} \|\widetilde{\Lambda}(\boldsymbol{y}, \boldsymbol{y}^*)\|_k, \tag{33}$$

to obtain $\widehat{\boldsymbol{y}}$ that satisfies

$$\|\widehat{\boldsymbol{y}} - \boldsymbol{y}\|_\infty \leq \varepsilon. \tag{34}$$

The norm $\|\cdot\|_k$ is defined as $\|\cdot\|_k = \sum_{i=1}^k \sigma_i(\cdot)$, and is known as *Ky Fan* k-norm. For any continuous linear operator in Hilbert spaces, the Ky Fan 1-norm corresponds to the usual operator norm equal to the largest singular value of the operator. The value of ε has to be small enough, depending on the size of the inclusion $|D|$ and on the jumps of the background coefficient. At the discretization level, one can use also the *Frobenius norm*, that takes into account all the singular values including the smallest ones.

The problem (33) is an ill-posed inverse problem over the parameter space Γ, which dimension can be very large. If more than one measurement of the operator Λ are available, *i.e.* $M > 1$, it is possible to exploit this further information solving

$$\widehat{\boldsymbol{y}} = \underset{\boldsymbol{y}^* \in \Gamma}{\operatorname{argmin}} \ \underset{1 \leq m \leq M}{\min} \|\widetilde{\Lambda}(\boldsymbol{y}_m, \boldsymbol{y}^*)\|_k, \tag{35}$$

so that the objective function contains more points of minima displaced in Γ, and the optimization algorithm can detect more easily one of them which satisfies (34), being $\mathbf{y}$ one among the M realizations that generated the M measurements. We will discuss in the numerical section how to efficiently solve problems (33) and (35).

3.1. The Factorization Method in the case of arbitrary measurements

In the case of random background with arbitrary measurements, we propose two versions of the FM.

The first version of the FM that we present is an optimized variant (Algorithm 2) where the background is reconstructed by means of an optimization approach. This optimization is mandatory whenever only one measurement or few measurements of the operator Λ are available. The additional operations w.r.t. Algorithm (1) concern the approximation of the solution $\widehat{\boldsymbol{y}}$ of the optimization problem (33) when only one measurement of Λ is available, or (35) when more than one measurement are available. The second version is named pure variant of the FM (Algorithm 3), because the final imaging reconstruction is a weighted linear combination of intermediate imaging reconstructions, each one obtained without any attempt to reconstruct the background. The approximation of the solution of problem (35) satisfying the convergence criterion (34) within a tolerance ε arbitrarily small is found by means of a sampling approach, rather than by optimization. This variant becomes attractive only when many measurements are available.

Algorithm 2 The optimized Factorization Method in random background (arbitrary measurements)

Sample the region of B to be probed with a set of points $\mathcal{P} = \{\boldsymbol{\xi}_j\}_{j=1}^P$,
Choose the initial guess $\widehat{\boldsymbol{y}}^{(i)} \in \Gamma$, $i = 0$,
repeat
    Compute $\widehat{\boldsymbol{y}}^{(i+1)}$ performing one or several steps in the optimization procedure for solving problem (33) with initial guess $\widehat{\boldsymbol{y}}^{(i)}$.
    for $\boldsymbol{\xi}$ in the set $\mathcal{P}$ **do**
        solve problem (5) with $\sigma_B = \sigma_B(\cdot, \widehat{\boldsymbol{y}}^{(i)})$ to find its solution $N(\cdot, \boldsymbol{\xi}, \widehat{\boldsymbol{y}}^{(i)})$,
        compute $l_{\boldsymbol{\xi}}^k(\widehat{\boldsymbol{y}}^{(i)})$ from $N(\cdot, \boldsymbol{\xi}, \widehat{\boldsymbol{y}}^{(i)})$ using (7),
        use $l_{\boldsymbol{\xi}}^k(\widehat{\boldsymbol{y}}^{(i)})$ to compute the indicator $C(\boldsymbol{\xi})$ in (22),
        plot $\boldsymbol{\xi} \mapsto C(\boldsymbol{\xi})$,
    end for
    $i \leftarrow i + 1$
until $\left(\text{the background is NOT reconstructed in } C(\boldsymbol{\xi})\right)$ OR $\left(\text{i} \geq \text{maxit}\right)$.

To set up an easy notation, we consider only the parametrization (26) of the coefficient σ_B with the vector $\mathbf{d}$. The same idea can be applied with any parametrization of σ_B. Define the l^∞ norm of an N-dimensional vector v, weighted w.r.t. the N-dimensional vector $\mathbf{d}$ as $\|\mathbf{v}\|_{\infty,\mathbf{d}} = \max\{d_1 v_1, \ldots, d_N v_N\}$. Given the values of N, M, ε and the vector $\mathbf{d}$, then the number T of realizations in the sampling procedure is chosen such that

$$\mathbb{P}\left[\min_{\substack{1 \leq m \leq M \\ 1 \leq t \leq T}} \|\boldsymbol{y}_m - \widehat{\boldsymbol{y}}_t\|_{\infty,\mathbf{d}} \leq \varepsilon\right] \geq 0.99. \tag{36}$$

Note that ε in (36) plays the same role as in (34). If the dispersion vector $\mathbf{d}$ has components all equal to $d > 0$, so that the dispersion is the same for all the components of the random variable $\mathbf{Y}$, then (36) can be rewritten with the usual l^∞ norm as

$$\mathbb{P}\left[\min_{\substack{1 \leq m \leq M \\ 1 \leq t \leq T}} \|\boldsymbol{y}_m - \widehat{\boldsymbol{y}}_t\|_\infty \leq \varepsilon\, d^{-1}\right] \geq 0.99. \tag{37}$$

In the pure FM T is choosen such that (36) is satisfied, and this allows to obtain with 99% probability an approximation of one of the realizations that generated the measurements, within a tolerance ε. In this way the optimization of problem (35) can be avoided. Note that, given M, N, d and ε, condition (37) states how to choose T such that the pure FM detects the inclusions with at least 99% probability. In Section 6.2 the calibration of ε is discussed and the value of T such that condition (37) holds is calculated for some values of M, N, d, ε.

Looking at Algorithms 2 and 3, it is clear that the most computationally expensive part of these two variants of the FM consists in the repetitive evaluation of Λ_0, for many realizations of the random variable $\mathbf{Y}$. In Algorithm 2 this operation is hidden inside

---

Algorithm 3 The pure Factorization Method in random background (arbitrary measurements)

    Collect M measurements $\Lambda(\boldsymbol{y}_1), \ldots, \Lambda(\boldsymbol{y}_M)$,

    Sample the region of B to be probed with a set of points $\mathcal{P} = \{\boldsymbol{\xi}_j\}_{j=1}^P$,

    Sample T realizations $\widehat{\boldsymbol{y}}_1, \ldots, \widehat{\boldsymbol{y}}_T \overset{\text{iid}}{\sim} \rho$ of the random variable $\mathbf{Y}$,

    $i = 1$,

    repeat

        Compute $F_{mi} = \|\Lambda(\boldsymbol{y}_m) - \Lambda_0(\widehat{\boldsymbol{y}}_i)\|_k$, $\forall m$ and $m_i = \text{argmin}_{m=1,\ldots,M} F_{mi}$,

        for $\boldsymbol{\xi}$ in the set $\mathcal{P}$ **do**

            solve problem (5) with $\sigma_B = \sigma_B(\cdot, \widehat{\boldsymbol{y}}^{(i)})$ to find its solution $N(\cdot, \boldsymbol{\xi}, \widehat{\boldsymbol{y}}^{(i)})$,

            compute $l_{\boldsymbol{\xi}}^k(\widehat{\boldsymbol{y}}^{(i)})$ from $N(\cdot, \boldsymbol{\xi}, \widehat{\boldsymbol{y}}^{(i)})$ using (7),

            use $l_{\boldsymbol{\xi}}^k(\widehat{\boldsymbol{y}}^{(i)})$ and the SVD decomposition of $\widetilde{\Lambda}(\boldsymbol{y}_{m_i}, \widehat{\boldsymbol{y}}_i)$ to compute $\|g_{\boldsymbol{\xi}}^k(\boldsymbol{y}_{m_i}, \widehat{\boldsymbol{y}}_i)\|_{L^2(\partial B)}$,

            use $\|g_{\boldsymbol{\xi}}^k(\boldsymbol{y}_{m_i}, \widehat{\boldsymbol{y}}_i)\|_{L^2(\partial B)}$ to compute the indicator $C_i(\boldsymbol{\xi})$ in (22),

            update $C(\boldsymbol{\xi}) \leftarrow C(\boldsymbol{\xi}) + C_i(\boldsymbol{\xi}) \exp\left(-\frac{(\min_{1\le j\le i} F_{m_j j})}{F_{m_i i}}\right)$,

            plot $\boldsymbol{\xi} \mapsto C(\boldsymbol{\xi})$,

        end for

        $i \leftarrow i+1$

    until $\left(\text{the background is NOT reconstructed in } C(\boldsymbol{\xi})\right)$ OR $\left(\text{i} \ge \text{T}\right)$.

---

the optimization step, where point-wise evaluations of Λ_0 are needed. The number of evaluations of Λ_0 to achieve an accurate approximation of the solution of problems (33) and (35) can be considerably reduced by means of polynomial approximation [16, 17] of problem (2) with the random coefficient (25), which defines the operator Λ_0.

3.2. The Factorization Method in the case of paired measurements

When a pair of measurements of Λ and Λ_0 is available, *i.e.* the measurements are generated from the same realization $\boldsymbol{y}$ of the random variable $\mathbf{Y}$, then we can build straightforwardly the operator $\widetilde{\Lambda}$ from (29). Since the value of the realization $\boldsymbol{y}$ that generated the measurements is unknown, we have to work with the sampling procedure to span the parameter space Γ looking for a good approximation of $\boldsymbol{y}$.

    Let $\{\mathbf{s}_t\}_{t=1}^T$ be T independent and identically distributed realizations of the random variable $\mathbf{Y}$ that are used to explore the parameter space Γ. We propose the following indicator function, that substitutes the one defined in (22):

$$\widehat{C}(\boldsymbol{\xi}) = \sum_{t=1}^T \frac{1}{\log_{10}\left(v_1(\boldsymbol{\xi}, \mathbf{s}_t) + v_2(\boldsymbol{\xi}, \mathbf{s}_t)\right)}, \tag{38}$$

In (38) the functions $v_k : (\boldsymbol{\xi}, \mathbf{y}) \in (D \times \Gamma) \mapsto v_k(\boldsymbol{\xi}, \mathbf{y}) : D \times \Gamma \to \mathbb{R}$ are defined as $v_k(\boldsymbol{\xi}, \mathbf{y}) := \|g_{\boldsymbol{\xi}}^k(\mathbf{y})\|_{L^2(\partial B)}$ and $g_{\boldsymbol{\xi}}^k(\mathbf{y})$ is again given by (19) but with $l_{\boldsymbol{\xi}}^p$ that depends on $\mathbf{y}$, as in (28). The indicator (38) is based on the sample mean estimator, which is

very sensitive to the outliers that correspond to the points where it diverges due to the presence of the inclusion. This variant of the FM that exploits the indicator function (38) is described in Algorithm (4). The number T of realizations to be evaluated with the FM has to be tuned according to the dimension N of the parameter space Γ.

Algorithm 4 The Factorization Method in random background (paired measurements)

    Sample the region of B to be probed with a set of points $\mathcal{P} = \{\boldsymbol{\xi}_j\}_{j=1}^{P}$,

    Sample T realizations $\mathbf{s}_1, \ldots, \mathbf{s}_T \overset{\text{iid}}{\sim} \rho$ of the random variable $\mathbf{Y}$,

    for $\boldsymbol{\xi}$ in the set $\mathcal{P}$ **do**

      for $t = 1, \ldots T$ **do**

        solve problem (5) with $\sigma_B = \sigma_B(\cdot, \mathbf{s}_t)$ to find its solution $N(\cdot, \boldsymbol{\xi}, \mathbf{s}_t)$,

        compute $l_{\boldsymbol{\xi}}^k(\mathbf{s}_t)$ from $N(\cdot, \boldsymbol{\xi}, \mathbf{s}_t)$ using (7),

        update the indicator $\widehat{C}(\boldsymbol{\xi})$ in (38) with $l_{\boldsymbol{\xi}}^k(\mathbf{s}_t)$,

      end for

      plot $\boldsymbol{\xi} \mapsto C(\boldsymbol{\xi})$.

    end for

---

4. Numerical tests featuring deterministic background

In this section we present several numerical tests to illustrate the capabilities of the Factorization Method in homogeneous and inhomogeneous but deterministic background. To show the results, we display the isolines of the indicator function $C(\boldsymbol{\xi})$ given by (22) A crucial issue is the tuning of the scale and the choice of the isovalue that represents the inclusion. In practice, this requires additional information on the value of the coefficient in the inclusions. In all the numerical tests we plot the indicator $C(\boldsymbol{\xi})$ in the domain B choosing an uniform coloring scale, such that the black color is associated to the zero value and the white color is associated to $\max_{\boldsymbol{\xi} \in B} C(\boldsymbol{\xi})$. Throughout the paper the space $\mathring{L}^2(\partial B)$ is discretized using the Fourier basis with 128 terms.

The domain B is always the unitary ball centered in $(0, 0)$. The sampling points consist of a 50×50 uniform grid over the square $[-1, 1] \times [-1, 1]$. In the FM we use only the points that fall 0.05 farther from ∂B. In the testcases with small inclusions the resolution is increased to 100×100. The dashed purple line always marks the exact geometry of the inclusion(s). The value of the coefficient that identifies the inclusion is always set to $\sigma_D = 0.001$, although any value that satisfies Assumption 1 is allowed.

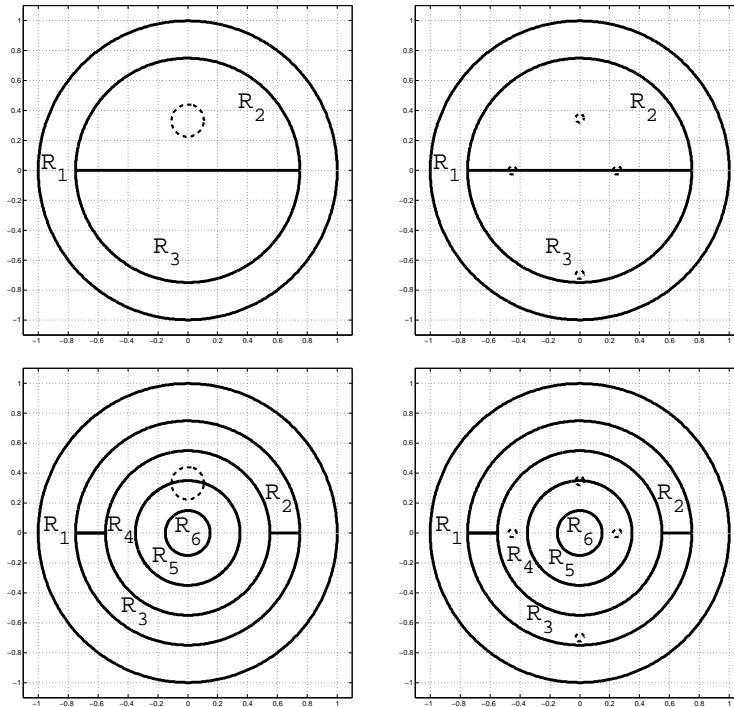We focus on two configurations of the background σ_B:

- (E) the union of two semicircular regions,
- (U) the union of five anular regions.

The inclusion(s) can be configured as

- (N) a circular inclusion with radius 0.1 centered in $(0, 0.33)$,

- (S) four small circular inclusions with radius 0.0275.

Combining each configuration of the background with each configuration of the inclusions we obtain the four configurations EN, ES, UN, US depicted in Fig. 3.

Fig. 3. Geometries of the regions in the background and displacement of the inclusions (in dashed line). Top-left: configuration EN. Top-right: configuration ES. Bottom-left: configuration UN. Bottom-right: configuration US.

4.1. The homogeneous case

We begin to apply the Factorization Method to the EIT problem with an homogeneous deterministic coefficient $\sigma_B \equiv 1$. Many numerical results in the literature show the potentiality of the method. The testcases are named as

- testcase hN: inclusion configuration N with $m_i = 1$, $i = 1, \dots, r$, in (24),
- testcase hS: inclusion configuration S with $m_i = 1$, $i = 1, \dots, r$, in (24).

With this choice of **m** the background configurations E and U become identical. Fig. 4 shows the results obtained with the inclusion configurations N and S, displaying the coloring of the indicator $C(\boldsymbol{\xi})$ in the domain B. In both cases, the reconstructions are very accurate and the shape and location of the inclusions are clearly detected.

4.2. The inhomogeneous case

We now proceed to present the results concerning the inhomogeneous deterministic coefficient σ_B. In this case the Factorization Method is described in Algorithm 1. As
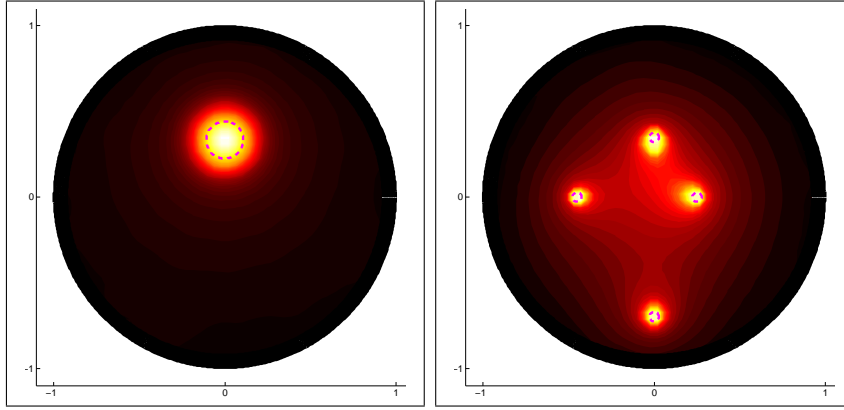
Fig. 4. Coloring of $C(\boldsymbol{\xi})$. Left: hN, $\gamma = 10^{-2}$. Right: hS, $\gamma = 5 \cdot 10^{-3}$.

will be explained in the next section, we pick the background coefficient equal to one in the region R_1 that is accessible to the boundary. In Fig. 5 and Fig. 6 we present the results obtained when applying the Factorization Method in the following testcases,

- testcase i1EN: configuration EN with $\boldsymbol{m} = [1, 5, 0.5]$ in (24),
- testcase i1ES: configuration ES with $\boldsymbol{m} = [1, 5, 0.5]$ in (24),

to achieve one order of magnitude jumps between different regions, or chosen as

- testcase i2EN: configuration EN with $\boldsymbol{m} = [1, 10, 0.1]$ in (24),
- testcase i2ES: configuration ES with $\boldsymbol{m} = [1, 0.1, 10]$ in (24),

to achieve two orders of magnitude jumps. Next, in Fig. 7 and Fig. 8 we present the
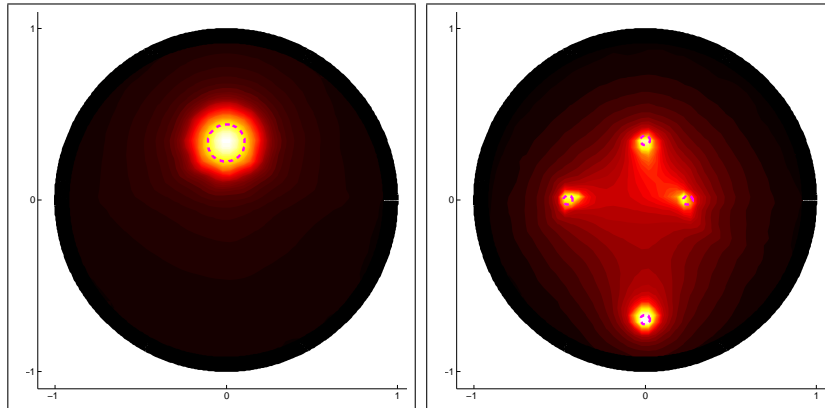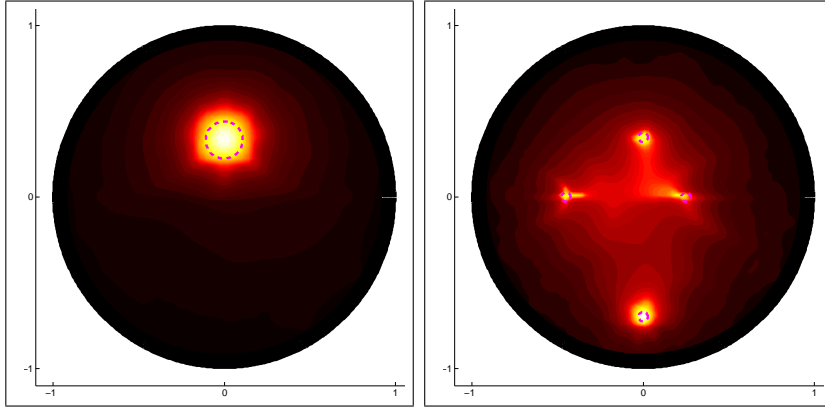

Fig. 5. Coloring of $C(\boldsymbol{\xi})$. Left: i1EN, $\gamma = 10^{-2}$. Right: i1ES, $\gamma = 7 \cdot 10^{-3}$.

results of the following testcases,

- testcase i1UN: configuration UN with $\boldsymbol{m} = [1, 5, 1, 5, 0.5, 0.5]$ in (24),
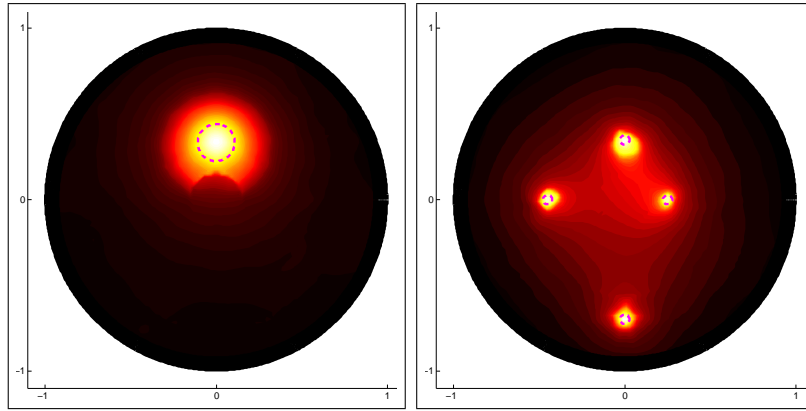- testcase i1US: configuration US with $\boldsymbol{m} = [1, 5, 1, 0.5, 1, 0.5]$ in (24),

to achieve one order jumps between different regions, or set as

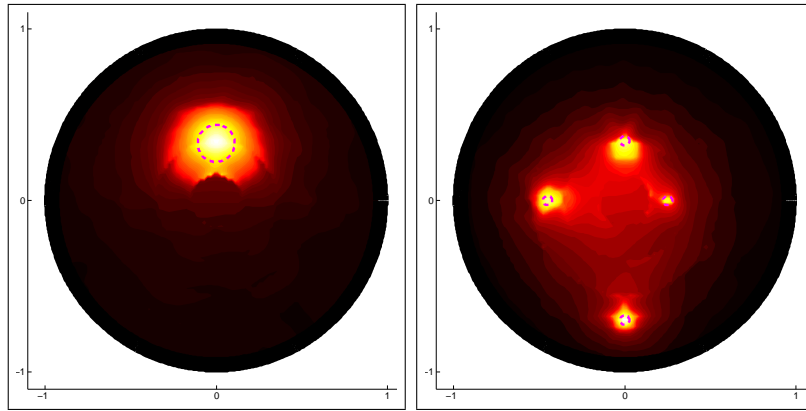- testcase i2UN: configuration UN with $\boldsymbol{m} = [1, 10, 1, 10, 0.1, 0.1]$ in (24),

Fig. 6. Coloring of $C(\boldsymbol{\xi})$. Left: i2EN, $\gamma = 10^{-2}$. Right: i2ES, $\gamma = 10^{-2}$.

- testcase i2US: configuration US with $\boldsymbol{m} = [1, 10, 1, 0.1, 1, 0.1]$ in (24),

to achieve two orders jumps. The quality of the reconstructions with jumps of one

Fig. 7. Coloring of $C(\boldsymbol{\xi})$. Left: i1UN, $\gamma = 5 \cdot 10^{-2}$. Right: i1US, $\gamma = 5 \cdot 10^{-3}$.

Fig. 8. Coloring of $C(\boldsymbol{\xi})$. Left: i2UN, $\gamma = 5 \cdot 10^{-2}$. Right: i2US, $\gamma = 10^{-2}$.

order of magnitude in Fig. 5 and Fig. 7 is the same as the quality in Fig. 4 with the

homogeneous background. See also many other numerical tests in [21], also with more general nonlinear inhomogeneous background coefficients.

When the order of magnitude of the jumps increases to two, the effect of the jump in the background coefficient becomes visible in the reconstruction, as in Fig. 8–left. Nonetheless the inclusion is still accurately detected. In Fig. 6–right we observe that the inclusions on the interface where the coefficient jumps are still detected, albeit with a fainter intensity of the indicator $C(\boldsymbol{\xi})$. The same occurs in Fig. 8–right with the most inner inclusion. All the four small inclusions are detected, but the method would hardly inspect the presence of additional inclusions inside their convex envelope. See also [21], where a test with ten small inclusions is performed.

We can conclude that the Factorization Method is able to accurately detect the shape and location of all the inclusions, when the jumps in the background are up to two orders of magnitude.

5. Numerical tests with one measurement featuring random background

In this section we present some numerical tests with random background, in the arbitrary measurements and paired measurements cases. We are interested in large variations of the background coefficient σ_B, and therefore we parametrize it with the exponential model (27) so that the coefficient jumps by two orders of magnitude in each one of the r regions, or

$$\sigma_B(\mathbf{x}, \mathbf{Y}) = \sum_{i=1}^{r} 0.5 \cdot 10^{Y_i} \, \mathbb{I}_{R_i}(\mathbf{x}), \quad \mathbf{x} \in B, \quad \mathbf{Y} \in \Gamma = [-0.5, 0.5]^r, \qquad (39)$$

to have one order jumps.

Usually in the problem of EIT the boundary is accessible. This would allow to directly recover the value of the realization of the random variable Y_1 that generated the voltage and current, corresponding to the observation of $\widetilde{\Lambda}$. As a consequence, the value of σ_B in R_1 could be retrieved, and the starting problem could be reduced to a problem with deterministic coefficient in R_1. For this reason, we will choose σ_B equal to 1 in R_1 and random only in $\Omega \setminus R_1$. In this way, the parameter space Γ in the parametrizations (26), (39), (27) has to be dimensionally reduced by one, so that its dimension in practice becomes $N = r - 1$.

We proceed now to present several numerical tests performed with the optimized FM (Algorithm 2) in the case of one arbitrary measurement, and with the FM of Algorithm (4) in the case of one paired measurement.

5.1. The optimized Factorization Method with one arbitrary measurement.

To show the capabilities of the proposed approach we set up three testcases, with an increasing difficulty in the optimization operations. We choose the following testcases featuring a random background:

- testcase aEN2: configuration EN with two orders jumps in the background coefficient defined in (27). The parameter space is $\Gamma = [0.1, 10]^2$. The measurement of $\Lambda(\boldsymbol{y})$ is generated by the realization $\boldsymbol{y} = (8.3567, 0.3558)$.

- testcase aES2: configuration ES with two orders jumps in the background coefficient defined in (27). The parameter space is $\Gamma = [0.1, 10]^2$. The measurement of $\Lambda(\boldsymbol{y})$ is generated by the realization $\boldsymbol{y} = (4.5, 0.75)$.

- testcase aUN1: configuration UN with one order jump in the background coefficient defined in (39). The parameter space is $\Gamma = [0.5, 5]^5$. The measurement of $\Lambda(\boldsymbol{y})$ is generated by the realization $\boldsymbol{y} = (4.4950, 1.3450, 0.9450, 3.3450, 0.6240)$.

The testcase aEN2 is a standard configuration, with a not too small inclusion and a two-dimensional parameter space Γ. The testcase aES2 is more challenging than testcase aAS2, because the inclusions have a smaller diameter and their presence is more easily obfuscated by the variations of the random background. Lastly, in testcase aUN1 we treat an ill-posed optimization problem over a five-dimensional parameter space, and the limits of the optimization approach are highlighted.
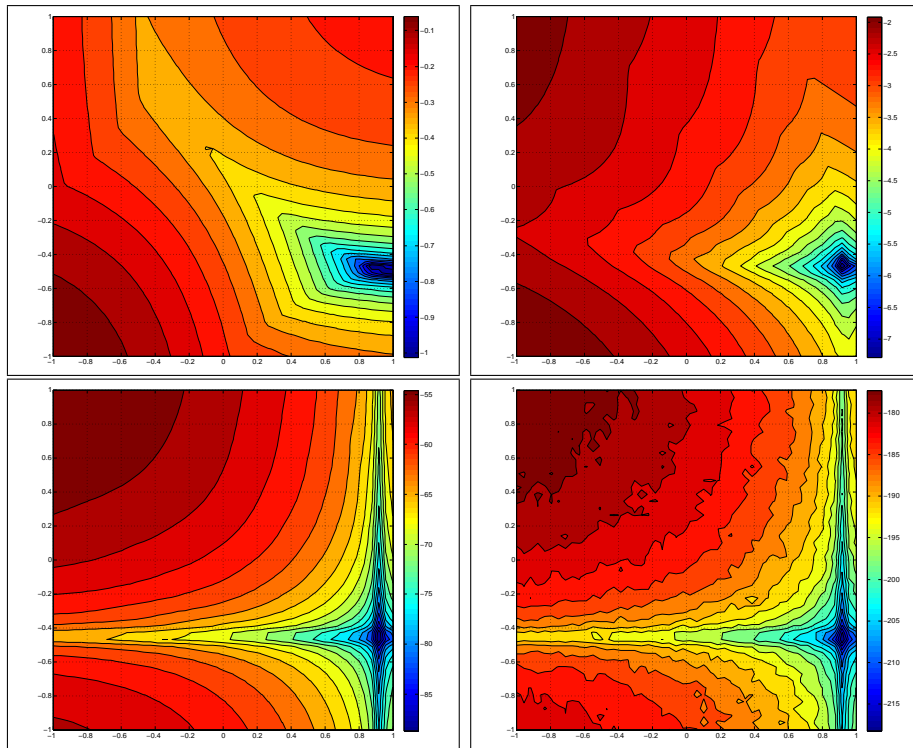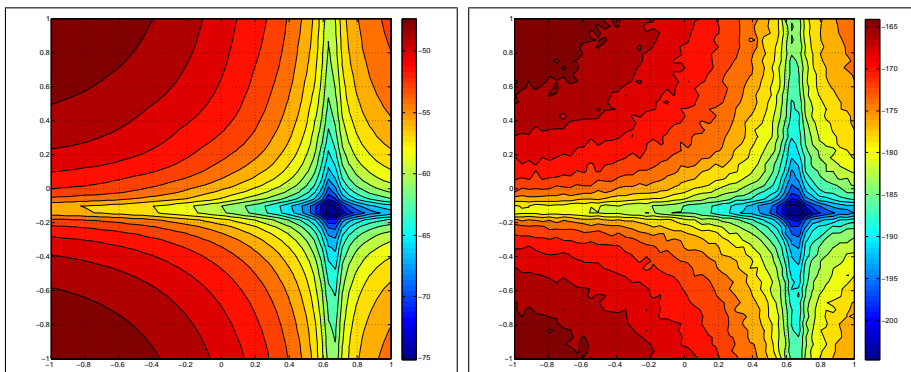

Fig. 9. Testcase aEN2. Function q_k over the parameter space Γ in log-log scale. Top-left: $k = 1$. Top-right: $k = 5$. Bottom-left: $k = 32$. Bottom-right: $k = 64$. The realization $\boldsymbol{y} = (8.3567, 0.3558)$ corresponds to the point of global minima $(0.9220, -0.4488)$ in log-log scale.

From a computational standpoint, the optimization of the Ki Fan k-norm $\| \cdot \|_k$ can be equivalently replaced by the optimization of the real-valued operator $q_k(\cdot) = \sum_{i=1}^{k} \log \sigma_i(\cdot)$, which has the same points of minima as $\| \cdot \|_k$. In Figs. 9, 10 and 11

we display the function q_k evaluated over the parameter space Γ in the testcases aEN2 and aES2, for some values of k. As explained in section 3, the solution of problem (33) that corresponds to the point of global minima is the realization $\boldsymbol{y}$ that generated the measurement of $\Lambda(\boldsymbol{y})$. The higher the value of k, and the steeper the objective function becomes, because more singular values are taken into account. Moreover, when k increases the objective function shows a product structure that suggests the use of *Alternating Minimization*. When Γ is two-dimensional, we present the numerical results only using a global optimization approach, although we observed that the Alternating Minimization allows to reduce the overall computational cost.

When $\Gamma = [0.5, 5]^5$, the global optimization approach converges to the correct solution in the subspace of the parameter space associated to the three outer regions, but then gets stuck into local minima when exploring the two most inner regions. Alternating Minimization converges even more easily, but still gets stuck into local minima whenever the initial data of the two most inner regions is not close enough to the exact solution. One possibility is to initialize with different initial data the optimization procedure, but since the parameter space is very large this turns out to be very costly. Therefore, we think that the optimization procedure could still be employed effectively but on problem (35) with more than one measurement of Λ and resizing the range of variation of the random variables of the most inner regions. For example, when Y_5, Y_6 deviate only 25% from their mean values the alternating minimization always easily finds one of the points of minima of problem (35). Some test with many measurements are presented in Section 6.

Fig. 10. Testcase aES2. Function q_k over the parameter space Γ in log-log scale. Left: $k = 32$. Right: $k = 64$. The realization $\boldsymbol{y} = (4.5, 0.75)$ corresponds to the point of global minima $(0.6532, -0.1249)$ in log-log scale.

To solve problem (33) we choose a derivative-free approach, since $\partial_{\boldsymbol{y}^*} \|\widetilde{\Lambda}(\boldsymbol{y}, \boldsymbol{y}^*)\|_k$ is not available. We employ the well-known Melder-Mead method [24] to perform a constrained optimization of the objective function q_k over the whole parameter space Γ.

In testcase aEN2 the method converged in less than 100 iterations to the solution $\widehat{\boldsymbol{y}}$ of problem (33) within an accuracy $\varepsilon = 10^{-4}$ in (34), for several different choices of the initial point in the parameter space. The number of evaluations of Λ_0 has always been less than three times the number of iterations.
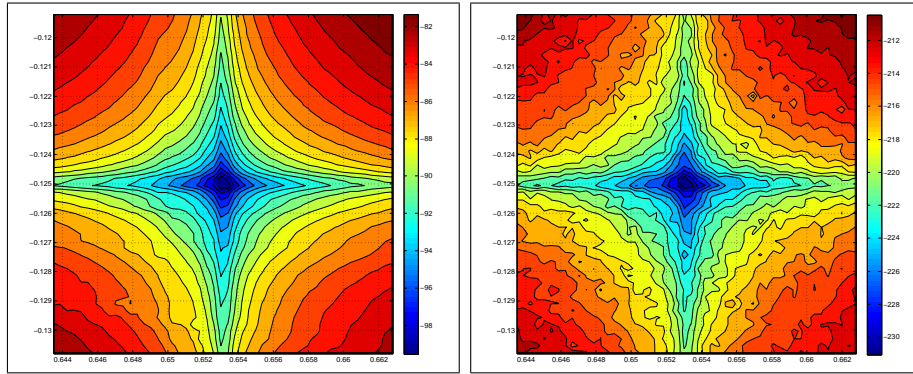
Fig. 11. Testcase aES2. Same as Fig. 10 but zoomed in a neighbourhood of the point of global minima $(0.6532, -0.1249)$. Function q_k over the parameter space Γ in log-log scale. Left: $k = 32$. Right: $k = 64$.

In testcase aES2 the method converged in less than 100 iterations to the solution $\widehat{\boldsymbol{y}}$ of problem (33) with an accuracy $\varepsilon = 10^{-3}$, for several different choices of the initial point in the parameter space. The evaluations of Λ_0 are more costly, because the finite element mesh has been chosen finer.
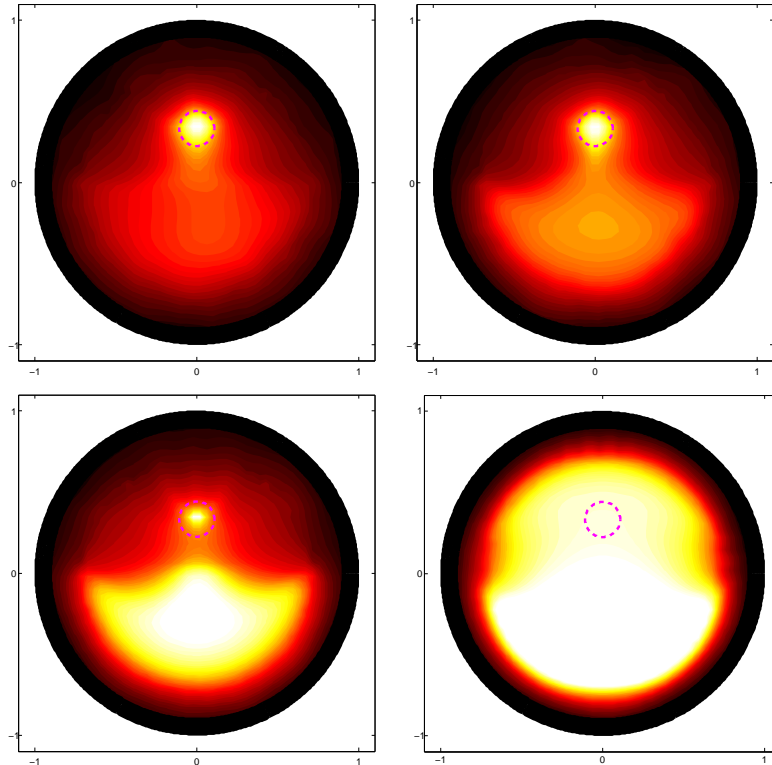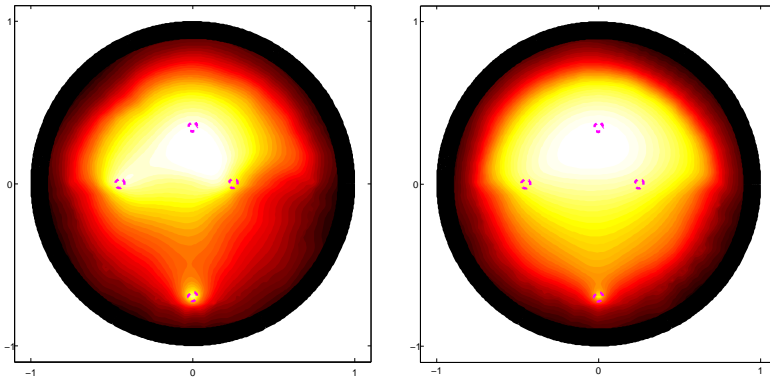

Fig. 12. Coloring of $C(\boldsymbol{\xi})$, aEN2, $\gamma = 10^{-2}$. Top-left: using the solution $\widehat{\boldsymbol{y}}$ of (33) with $\varepsilon = 0.00014$. Top-right: using the solution $\widehat{\boldsymbol{y}}$ of (33) with $\varepsilon = 0.001$. Bottom-left: using the solution $\widehat{\boldsymbol{y}}$ of (33) with $\varepsilon = 0.01$. Bottom-right: using the point $\widehat{\boldsymbol{y}} = (5.05, 5.05)$.

Once we obtain an approximation $\widehat{\boldsymbol{y}}$ of the solution of problem (33), we can apply the FM with the realization $\widehat{\boldsymbol{y}}$. In Fig. 12 we show the reconstructions obtained in

the testcase aEN2, with different values of ε. We solve problem (33) with the Ky Fan 5-norm with initial point $(0.1, 10)$, and after 76 iterations and 223 evaluations of Λ_0 the method converges to the solution $\widehat{\boldsymbol{y}} = (8.356653, 0.355660)$ such that the convergence criterion (34) is satisfied with $\varepsilon = 0.00014$. The corresponding reconstruction obtained is depicted in Fig. 12-top-left. The other Figs. 12-top-right and 12-bottom-left show the effect of using a less accurate realization $\widehat{\boldsymbol{y}}$ for different values of ε. Fig. 12-bottom-right is obtained using $\widehat{\boldsymbol{y}} = (5.05, 5.05)$, that is the expected value of the random variable $\boldsymbol{Y}$ over Γ, and yields a reconstruction where the inclusion is completely obfuscated by the contrast of the background.
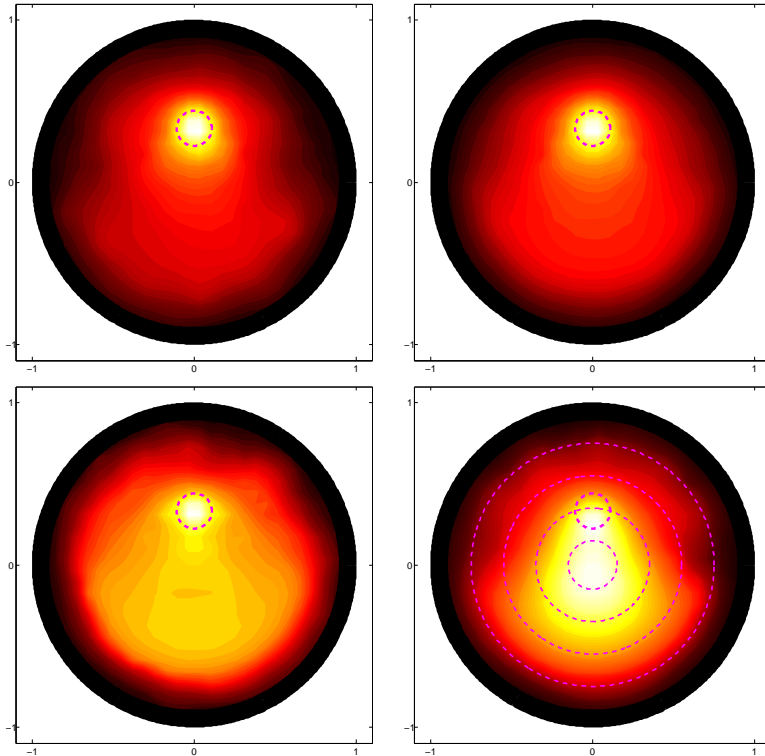

Fig. 13. Coloring of $C(\boldsymbol{\xi})$, aES2, $\gamma = 10^{-2}$. Left: using the solution $\widehat{\boldsymbol{y}}$ of (33) with $\varepsilon = 10^{-3}$. Right: using the solution $\widehat{\boldsymbol{y}}$ of (33) with $\varepsilon = 10^{-2}$.

As justified in section 3, when applying the FM with a realization $\widehat{\boldsymbol{y}}$ that is not enough accurate with respect to the criterion (34), the background begins to be detected in the reconstruction. This fact can be used to check a posteriori that the solution of problem (33) is accurate enough: if the region R_i of the background is sharply detected, then the ith component of the solution $\widehat{\boldsymbol{y}}$ of problem (33) is too inaccurate, and its accuracy needs to be improved. To achieve an improvement one can either utilize Alternating Minimization, or increase k or choose other types of optimization methods, *e.g.* Simulated Annealing or Global Pattern Search.

In Fig 13-left we show the reconstruction obtained in testcase aES2 using the solution $\widehat{\boldsymbol{y}}$ of problem (33) that satisfies (34) with $\varepsilon = 10^{-3}$. This solution was computed solving problem (33) with the Ky Fan 32-norm with initial point $(0.1, 10)$, and required 131 iterations and 312 evaluations of Λ_0.

Finally we present the testcase aUN1, that shows the limit of the optimization procedure with large variations of the coefficients. In Fig. 14 we show the results obtained for different values of ε: on top-left we show the reconstruction obtained when solving accurately problem (33) with $\varepsilon = 5 \cdot 10^{-4}$, on bottom-right we display the reconstruction obtained when the optimization of problem (33) is accurate with $\varepsilon = 10^{-2}$ only in the three most outer regions, but converged only up to $\varepsilon = 0.2$ in the subspace of Γ associated to the two most inner regions. As a result, the two most inner regions are detected as an inclusion.

Fig. 14. Coloring of $C(\boldsymbol{\xi})$, aUN1, $\gamma = 10^{-2}$. Top-left: using the solution $\widehat{\boldsymbol{y}}$ of (33) with $\varepsilon = 0.0005$. Top-right: using the solution $\widehat{\boldsymbol{y}}$ of (33) with $\varepsilon = 0.001$. Bottom-left: using the solution $\widehat{\boldsymbol{y}}$ of (33) with $\varepsilon = 0.01$. Bottom-right: using the solution $\widehat{\boldsymbol{y}}$ of (33) with $\varepsilon = 0.01$ in R_2, R_3, R_4 and $\varepsilon = 0.2$ in R_5, R_6.

In general, we observed that the global optimization over the whole five-dimensional parameter space is always successfully, when applied to testcases featuring small variations of the coefficients in the most inner regions, *e.g.* up to 25%. On the other side, when the starting point is not sufficiently close to the exact solution and the variations of the coefficients are of one order of magnitude in the two most inner regions, the global optimization over the five-dimensional parameter space got stuck into local minima. Clearly, this is a limitation of the proposed approach, and the availability of more than one measurement to facilitate the optimization seems required to overcome it.

5.2. The Factorization Method with one paired measurement

In the case of paired measurements, with the configurations EN and UN the inclusion is always easily detected, also when the background coefficient jumps by two orders of magnitude. Therefore, we will not present these results, but focus only on the more challenging configurations ES and US, again with two orders of magnitude jumps in the background coefficient. We consider the following testcases, to test the FM in the paired measurements case:

- testcase pES: configuration pES with σ_B defined in (27),
- testcase pUS: configuration pUS with σ_B defined in (27).

The results obtained are presented in Fig. 15 for the testcase pES, and in Fig. 16 for the testcase pUS. We use the indicator $\widehat{C}(\boldsymbol{\xi})$ in (38) with the number T of realizations
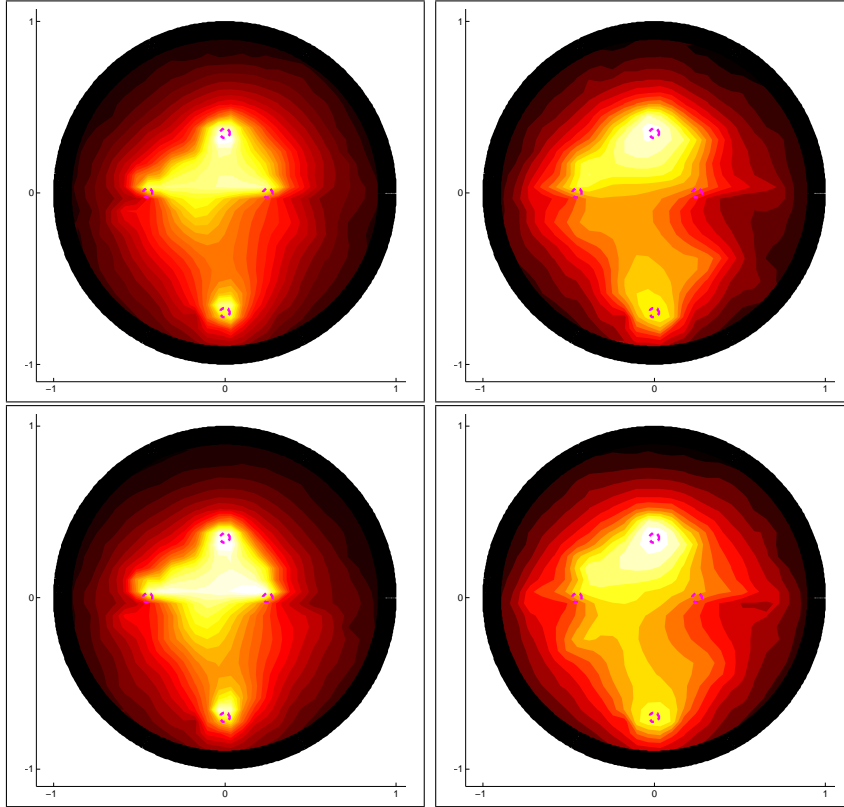
Fig. 15. Coloring of $\widehat{C}(\boldsymbol{\xi})$ with $T = 10$, pES, $\gamma = 5 \cdot 10^{-2}$. Top-left: $\sigma_B = (1, 0.5, 5)$. Top-right: $\sigma_B = (1, 5, 0.5)$. Bottom-left: $\sigma_B = (1, 0.1, 10)$. Bottom-right: $\sigma_B = (1, 10, 0.1)$.

chosen according to the number of regions r. We choose $T = 10$ when $r = 3$ and $T = 20$ when $r = 6$. Then we apply the FM when observing only one measurement of the random operator $\widetilde{\Lambda}$, generated from the unknown realization $\boldsymbol{y}$. The results are presented when "common" realizations are observed, *e.g.* $\sigma_B = (1, 5, 0.5)$ or $\sigma_B = (1, 0.26, 4.17, 0.89, 7.05, 0.16)$, and when "extremal" realizations are observed as well. We distinguish between "common" and "extremal" realizations in the following sense: an extremal realization lies on the boundary of the support of the random variable, *e.g.* $\sigma_B = (1, 10, 0.1)$ and $\sigma_B = (1, 10, 0.1, 0.1, 10, 10)$. If a realization is not extremal, than it is a "common" realization. Extremal realizations provide a worst-case benchmark for the FM.

With all the realizations observed, the FM detects at least three inclusions over four. The inclusion closest to the center of the domain is the hardest to detect. The reconstructions rely on the unique realization of the random operator $\widetilde{\Lambda}$, and this justifies its slight dependence on the particular realization observed. In spite of this, at least three inclusions are always sharply detected, but one is occasionally undetected.
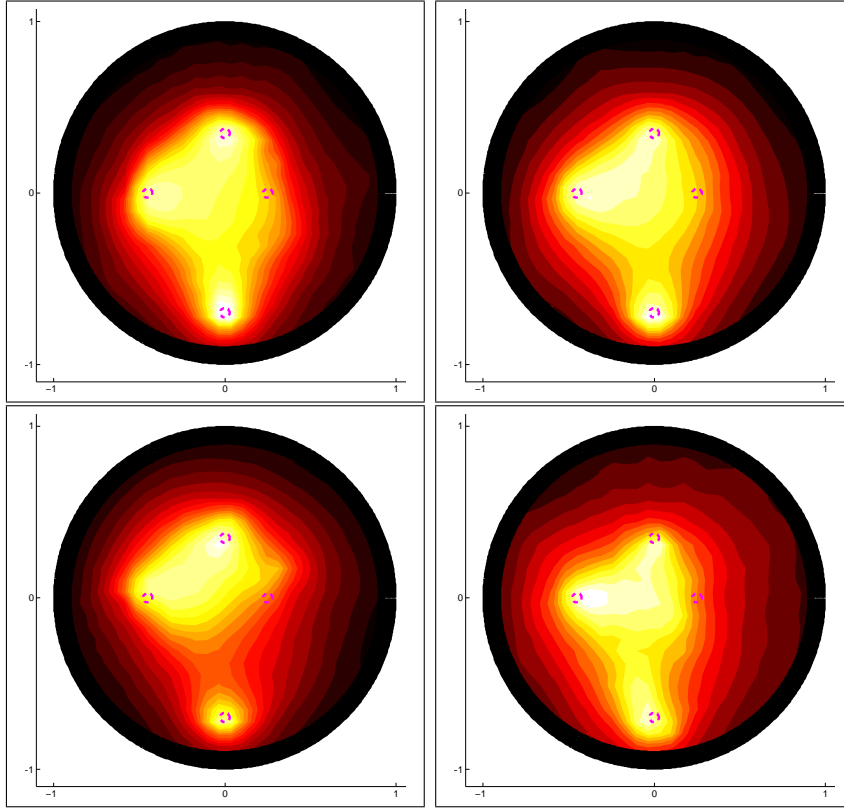
Fig. 16.   Coloring of $\widehat{C}(\boldsymbol{\xi})$ with $T = 20$, pUS, $\gamma = 5 \cdot 10^{-2}$.   Top-left: $\sigma_B = (1, 0.26, 4.17, 0.89, 7.05, 0.16)$.   Top-right: $\sigma_B = (1, 10, 0.1, 0.1, 10, 10)$.   Bottom-left: $\sigma_B = (1, 10, 1, 0.1, 1, 0.1)$. Bottom-right: $\sigma_B = (1, 0.1, 0.1, 10, 0.1, 10)$.

6. Numerical tests with many measurement featuring random background

6.1. The optimized Factorization Method with many arbitrary measurements.

As described previously, the optimization in problem (33) can be facilitated, optimizing problem (35) where additional measurements of $\Lambda(\boldsymbol{Y})$ are included. Fig. 17 shows the evaluation over Γ of the objective function of problem (35) with $\| \cdot \|_k$ replaced by $q_k(\cdot)$, in the testcases aEN2 and when four additional measurements are added to the one measurement of Λ available.

6.2. The pure Factorization Method with many arbitrary measurements.

Here we discuss some details about the application of the pure Factorization Method. The critical issue concerns the choice of ε. In Figs. 12-top-right, 13-left, 14-top-right several accurated reconstructions are obtained with $\varepsilon = 10^{-3}$ and much larger variations in the coefficient. Based on this observation, and on many other numerical experiments that we do not report, an accuracy $\varepsilon = 10^{-3}$ is always enough to clearly detect inclusions of normal size, *e.g.* with radius 0.1, when there are up to $r = 4$ regions, d is not larger than 0.125 and the vector **m** does not produce jumps in the coefficient larger than one
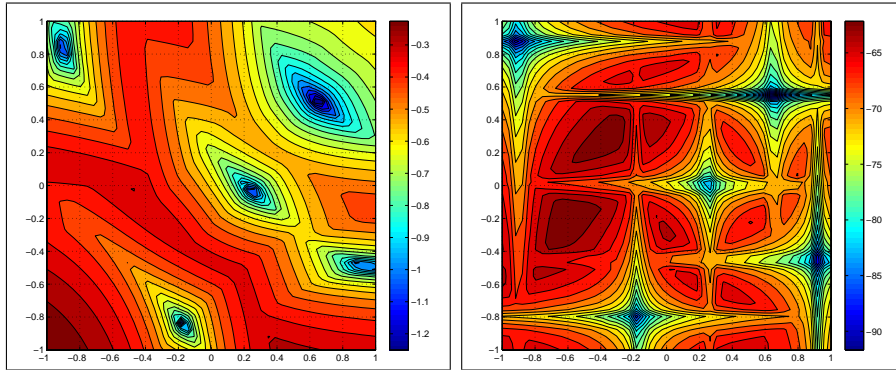
Fig. 17. Testcase aEN2 with 5 measurements of $\Lambda(\boldsymbol{Y})$. Evaluation over Γ in log-log scale of the objective function of problem (35), with $\|\cdot\|_k$ replaced by q_k. The realizations $\boldsymbol{y}_1, \boldsymbol{y}_2, \boldsymbol{y}_3, \boldsymbol{y}_4, \boldsymbol{y}_5$ correspond to the five points of minima. Left: $k = 1$. Right: $k = 32$.

order of magnitude. When interested in smaller inclusions, with more regions $r > 4$, or d and $\mathbf{m}$ that produce larger variations in σ_B, then also the value of ε has to be furtherly decreased.

Table 1 reports the number T of realizations needed to satisfy (36), for some values of M, N, d, $\varepsilon = 10^{-3}$, σ_B parametrized by (26) and d up to 0.125, yielding 25% variations in the coefficient. Note that this variation is much smaller than those treated in Figs. 12-top-right, 13-left, 14-top-right.

In Table 2 we report the value of T such that a condition analogous to (36) holds, but with the exponential parametrizations (39) and (27). The ranges of variations achieved with these parametrizations are the same as in Figs. 12-top-right, 13-left, 14-top-right.

	$d = 0.025$	$d = 0.05$	$d = 0.1$	$d = 0.125$
$M = 3$, $N = 2$ $(r = 3)$	1300	4500	15800	-
$M = 10$, $N = 2$ $(r = 3)$	400	1200	4500	7200
$M = 10$, $N = 3$ $(r = 4)$	9000	60000	-	-
$M = 25$, $N = 2$ $(r = 3)$	200	600	1900	2800
$M = 50$, $N = 2$ $(r = 3)$	100	300	1000	1600
$M = 50$, $N = 3$ $(r = 4)$	2000	14000	63000	133000

Table 1. Uncertainty Analysis. The value of T such that $\mathbb{P}[\min_{mt} \|\boldsymbol{y}_m - \widehat{\boldsymbol{y}}_t\|_\infty \leq \varepsilon \, d^{-1}] \geq 0.99$, given $\varepsilon = 10^{-3}$ and some values of N, M, d. Parametrization of σ_B by (26), where $\boldsymbol{y}_m, \widehat{\boldsymbol{y}}_t \in [-1,1]^N$. The dash advises for a larger value of M.

We remark that the value of T directly corresponds to the number of evaluations of the operator Λ_0 in points of the parameter space Γ. This evaluation can be performed very efficiently by means of polynomial approximation techniques.

	$[0.5, 5]$	$[0.1, 10]$
$M = 100$, $N = 1$ $(r = 2)$	40	70
$M = 100$, $N = 2$ $(r = 2)$	10800	36400
$M = 1000$, $N = 1$ $(r = 2)$	10	30
$M = 1000$, $N = 2$ $(r = 3)$	1300	4500

Table 2. Large variations. The value of T such that $\mathbb{P}[\min_{mt} \|\boldsymbol{y}_m - \widehat{\boldsymbol{y}}_t\|_\infty \leq \varepsilon] \geq 0.99$, given $\varepsilon = 10^{-3}$ and some values of N, M. Left column: one order of magnitude variations with the parametrization (39) of σ_B, where $\boldsymbol{y}_m, \widehat{\boldsymbol{y}}_t \in [0.5, 5]^N$. Right column: two orders of magnitude variations with the parametrization (27) of σ_B, where $\boldsymbol{y}_m, \widehat{\boldsymbol{y}}_t \in [0.1, 10]^N$.

7. Conclusions

In this paper we provided a numerical scheme to solve the Neumann dipole-like boundary value problem in inhomogeneous deterministic background. Then we employed this scheme to apply the FM to the problem of EIT in inhomogeneous deterministic and random background.

With any type of background the FM is able to detect the presence and location of one or many inclusions, and to supply information on their geometry. The quality of the reconstructions obtained in the inhomogeneous case is comparable to the quality of those in the homogeneous case, with jumps in the background up to two orders of magnitude.

When the background is random and the jumps are of two orders of magnitude, the inclusions are reconstructed at a lower accuracy. We provided three variants of the FM, based on the distinction between arbitrary and paired measurements of the random operator Λ. In the paired measurement case the FM always detects a normal or small inclusion. In presence of many inclusions those harder to detect could remain undetected. In the case of arbitrary measurements, the quality of the reconstruction depends on the accuracy ε of the criterion (34) when solving problem (33). We focused mainly on large variations of the coefficients, and showed that when the parameter space is low-dimensional the solution of problem (33) can be easily approximated up to a tolerance ε such that the FM is successful. When the dimension of the parameter space increases the optimization becomes challenging, in particular with large variations of the background coefficient. Another potentiality of the proposed approach, is the possibility to easily incorporate many measurements of the operator Λ in problem (35), which optimization can be a lot quicker than for problem (33) with only one measurement. Lastly we proposed a pure variant of the FM, that is particularly suited for uncertainty analysis and does not require the optimization step.

References

[1] Muller J L and Siltanen S. *Linear and Nonlinear Inverse Problems with Practical Applications.* SIAM Computational Science and Engineering, 2012.

[2] Borcea L. Addendum to: "Electrical impedance tomography" [Inverse Problems **18** (2002), no. 6, R99–R136; 1955896]. *Inverse Problems*, 19(4):997–998, 2003.

[3] Cheney M, Isaacson D, and Newell J C. Electrical impedance tomography. *SIAM Rev.*, 41(1):85–101 (electronic), 1999.

[4] Seppänen A, Vauhkonen M, Vauhkonen P J, Somersalo E, and Kaipio J P. State estimation with fluid dynamical evolution models in process tomography—an application to impedance tomography. *Inverse Problems*, 17(3):467–483, 2001.

[5] Guo Z and Zou Y. A review of electrical impedance techniques for breast cancer detection. *Medical Engineering & Physics*, 25(2):79 – 90, 2003.

[6] Astala K and Päivärinta L. Calderón's inverse conductivity problem in the plane. *Ann. of Math. (2)*, 163(1):265–299, 2006.

[7] Brown R M and Torres R H. Uniqueness in the inverse conductivity problem for conductivities with 3/2 derivatives in L^p, $p > 2n$. *J. Fourier Anal. Appl.*, 9(6):563–574, 2003.

[8] Alessandrini G. Stable determination of conductivity by boundary measurements. *Appl. Anal.*, 27(1-3):153–172, 1988.

[9] Lee J M and Uhlmann G. Determining anisotropic real-analytic conductivities by boundary measurements. *Comm. Pure Appl. Math.*, 42(8):1097–1112, 1989.

[10] Kirsch A and Grinberg N. *The factorization method for inverse problems*. Oxford University Press, 2008.

[11] Lechleiter A, Hyvönen N, and Hakula H. The factorization method applied to the complete electrode model of impedance tomography. *SIAM J. Appl. Math.*, 68(4):1097–1121, 2008.

[12] Hyvönen N, Hakula H, and Pursiainen S. Numerical implementation of the factorization method within the complete electrode model of electrical impedance tomography. *Inverse Probl. Imaging*, 1(2):299–317, 2007.

[13] Harrach B and Seo J K. Detecting inclusions in electrical impedance tomography without reference measurements. *SIAM J. Appl. Math.*, 69(6):1662–1681, 2009.

[14] Azzouz M, Hanke M, Oesterlein C, and Schilcher K. The factorization method for electrical impedance tomography data from a new planar device. *International Journal of Biomedical Imaging*, 2007.

[15] Hanke M and Schappel B. The factorization method for electrical impedance tomography in the half-space. *SIAM J. Appl. Math.*, 68(4):907–924, 2008.

[16] Babuška I, Tempone R, and Zouraris G E. Galerkin finite element approximations of stochastic elliptic partial differential equations. *SIAM J. Numer. Anal.*, 42(2):800–825, 2004.

[17] Cohen A, Devore R, and Schwab C. Analytic regularity and polynomial approximation of parametric and stochastic elliptic PDE's. *Anal. Appl. (Singap.)*, 9(1):11–47, 2011.

[18] Migliorati G, Nobile F, von Schwerin E, and Tempone R. Analysis of the discrete l^2 projection on polynomial spaces with random evaluations. *submitted. Available as MOX report 46-2011 at mox.polimi.it*, 2011.

[19] Brühl M. Explicit characterization of inclusions in electrical impedance tomography. *SIAM J. Math. Anal.*, 32(6):1327–1341 (electronic), 2001.

[20] Gebauer B and Hyvönen N. Factorization method and irregular inclusions in electrical impedance tomography. *Inverse Problems*, 23(5):2159–2170, 2007.

[21] Haddar H and Migliorati G. Numerical analysis of the factorization method for electrical impedance tomography in inhomogeneous medium. *INRIA RR-7801*, 2011, available at http://hal.inria.fr/hal-00641260.

[22] Haddar H and Kress R. Conformal mapping and impedance tomography. *Inverse Problems*, 26(7):074002, 18, 2010.

[23] Siltanen S, Mueller J, and Isaacson D. An implementation of the reconstruction algorithm of A Nachman for the 2D inverse conductivity problem. *Inverse Problems*, 16:681–699, 2000.

[24] Lagarias J C, Reeds J A, Wright M H, and Wright P E. Convergence properties of the Nelder-Mead simplex method in low dimensions. *SIAM Journal of Optimization*, 9(1):112 – 147, 1998.